Revisiting the Excited State Proton Transfer Dynamics in N-Oxide-Based Fluorophore: A Keto-Enol/Enolate Interplay to Detect Trace Water in Organic Solvents

Savita, Adarash Kumar Shukla, and Anupam Bhattacharya*
Department of Chemistry, Birla Institute of Technology and Science-Pilani (Hyderabad Campus), Hyderabad-500078, India.
E-mail: anupam@hyderabad.bits-pilani.ac.in; Tel: +91-40-66303522.

Supporting Information

Materials and Methods:

General procedure for UV and Fluorescence measurements:

All spectroscopic measurements were performed at room temperature. The protonated and deprotonated state was achieved by addition of 100 μM TFA and TEA in the solvent of interest. All spectroscopic measurements were made using a cuvette with 1 cm optical path length. A fresh stock solution of the probe (10 mM) was prepared in DMSO for the experiments on each day. All the experiments were performed in triplicates. Dry solvents Dioxane, Toluene, THF, DMSO, CH_2Cl_2, DMF, MeOH, CH_3CN (SRL, 99% anhydrous, water content 0.05%) and TEA(Triethyl amine) and TFA (Trifluoro acetic acid) were used as received. Milli Q water was used as obtained from the Millipore water filtration system. Water content in solvents was also detected using the Karl Fischer Titrator. For the steady-state spectra, solutions with 10 μM of HCQ in solvents were prepared unless specified. For all the fluorescence spectral measurements the slit width was kept 3 nm for both excitation and emission.

Synthetic route for HCQ:

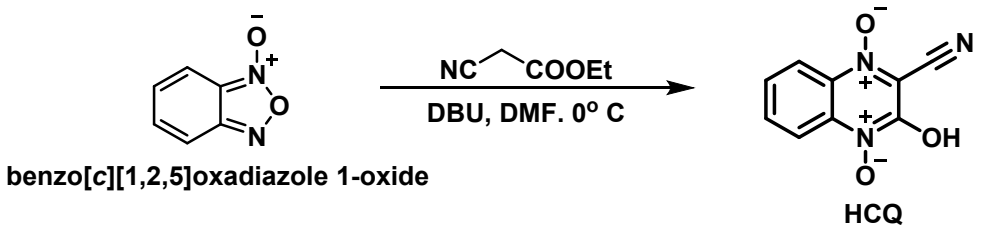

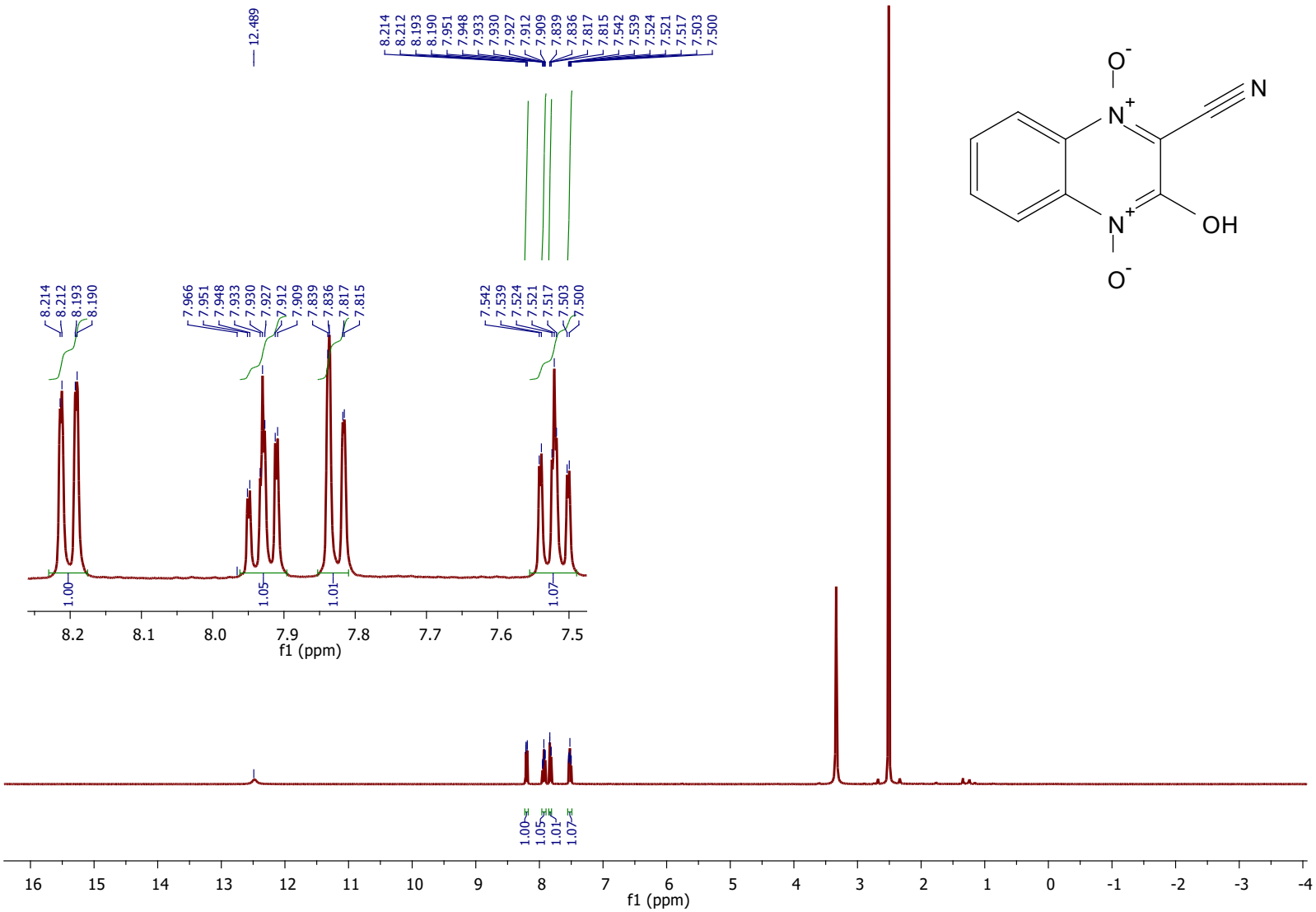

Figure S1(a). ^{1}H NMR spectrum of HCQ in DMSO-d_6

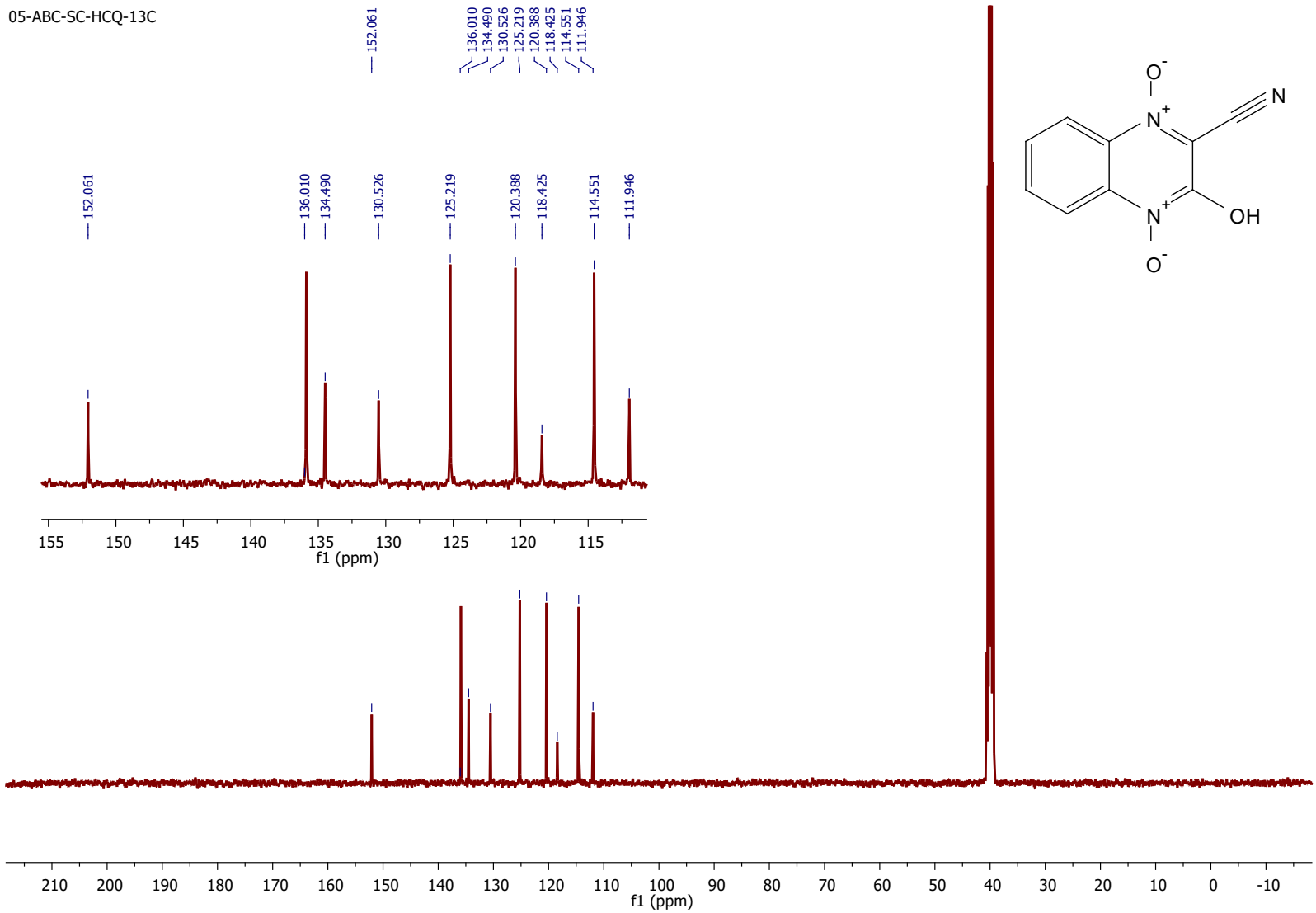

Figure S1(b). ^{13}C NMR spectrum of HCQ in DMSO-d_6.

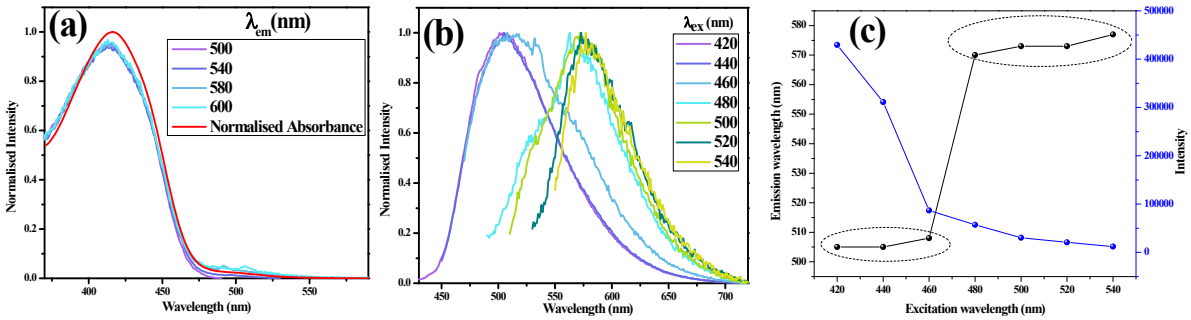

Figure S2(a). Normalised Absorption spectra; Normalised Excitation spectra with varying λ_{em} **(b)** Emission spectra with varying λ_{ex} and **(c)** Scatter plot for representing emission wavelength at maximum Intensity at varying excitation wavelength for HCQ (10 μM) in Toluene.

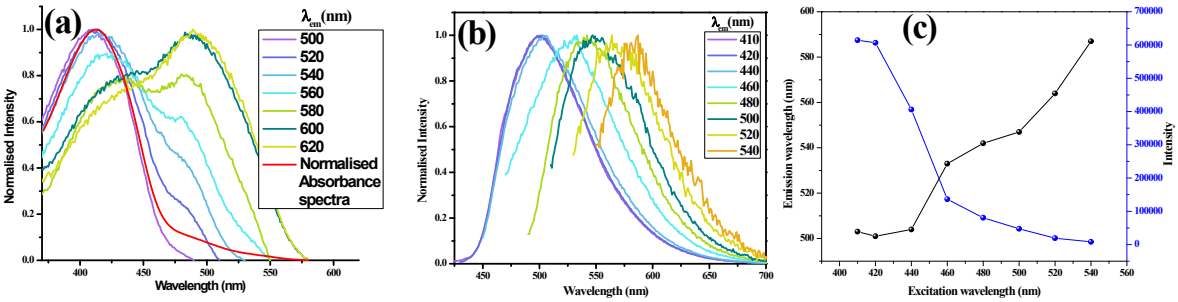

Figure S3(a). Normalised Absorption spectra; Normalised Excitation with varying λ_{em} **(b)** Emission spectra with varying λ_{ex} and **(c)** Scatter plot for representing emission wavelength at maximum Intensity at varying excitation wavelength for HCQ (10 μM) in Dioxane.

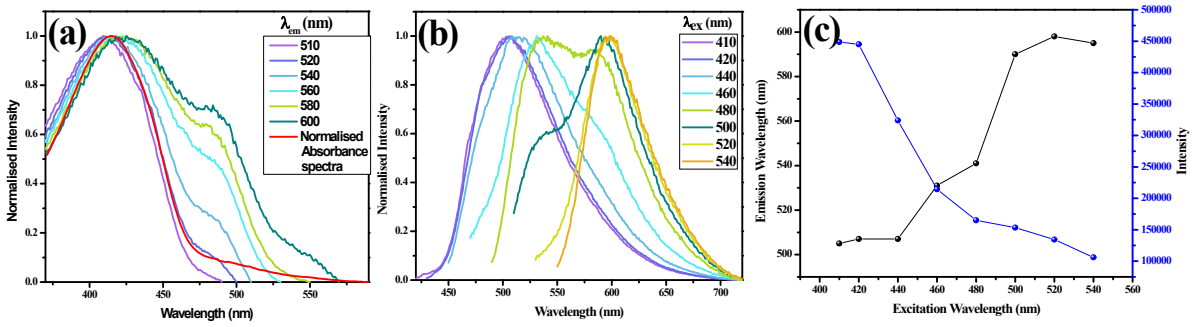

Figure S4(a). Normalised Absorption spectra; Normalised Excitation spectra with varying λ_{em} **(b)** Emission spectra with varying λ_{ex} and **(c)** Scatter plot for representing emission wavelength at maximum Intensity at varying excitation wavelength for HCQ (10 μM) in THF.

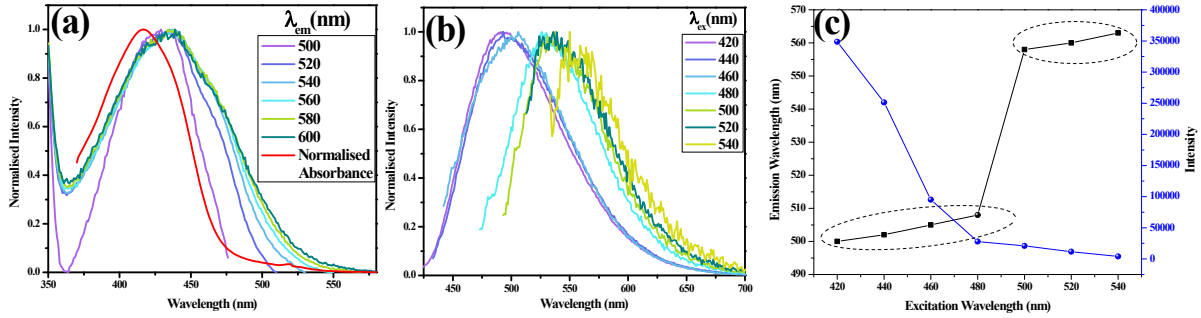

Figure S5(a). Normalised Absorption spectra; Normalised Excitation spectra with varying λ_{em} **(b)** Emission spectra with varying λ_{ex} and **(c)** Scatter plot for representing emission wavelength at maximum Intensity at varying excitation wavelength for HCQ (10 μM) in CH_2Cl_2.

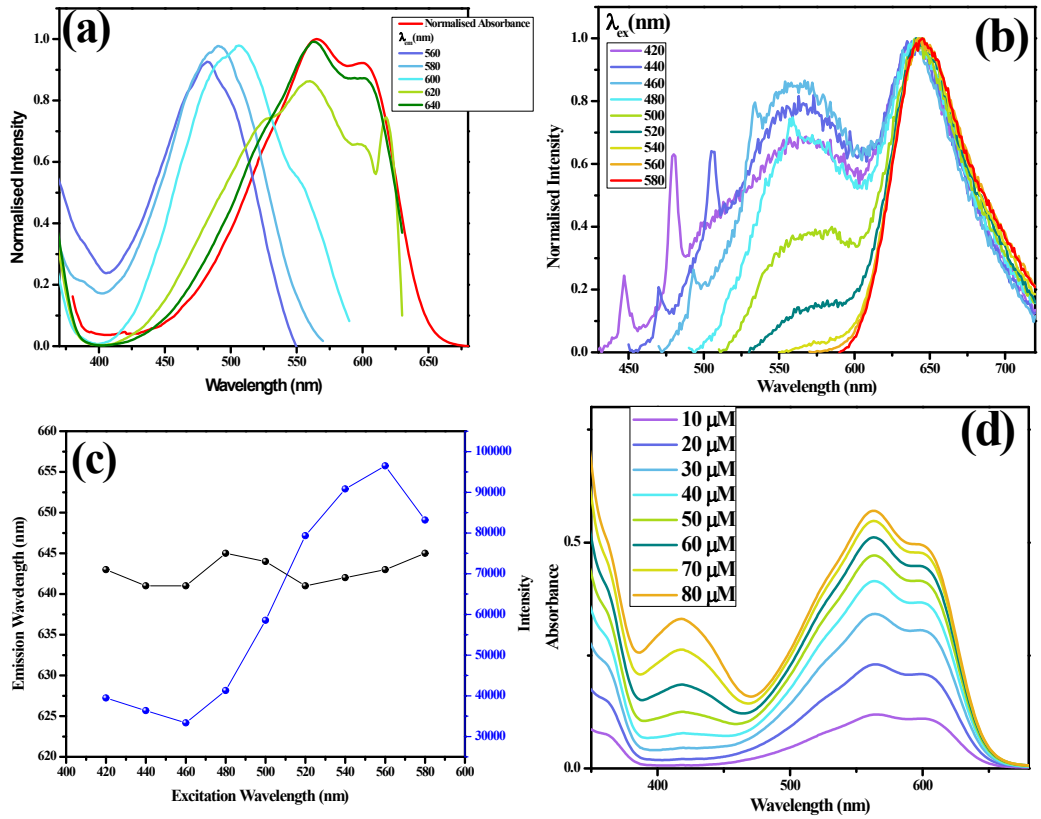

Figure S6(a). Normalised Absorption spectra; Normalised Excitation spectra with varying λ_{em} **(b)** Emission spectra with varying λ_{ex} and **(c)** Scatter plot for representing emission wavelength at maximum Intensity at varying excitation wavelength for HCQ (10 μM) in DMF **(d)** Absorbance spectra of HCQ with increasing concentration of HCQ in DMF

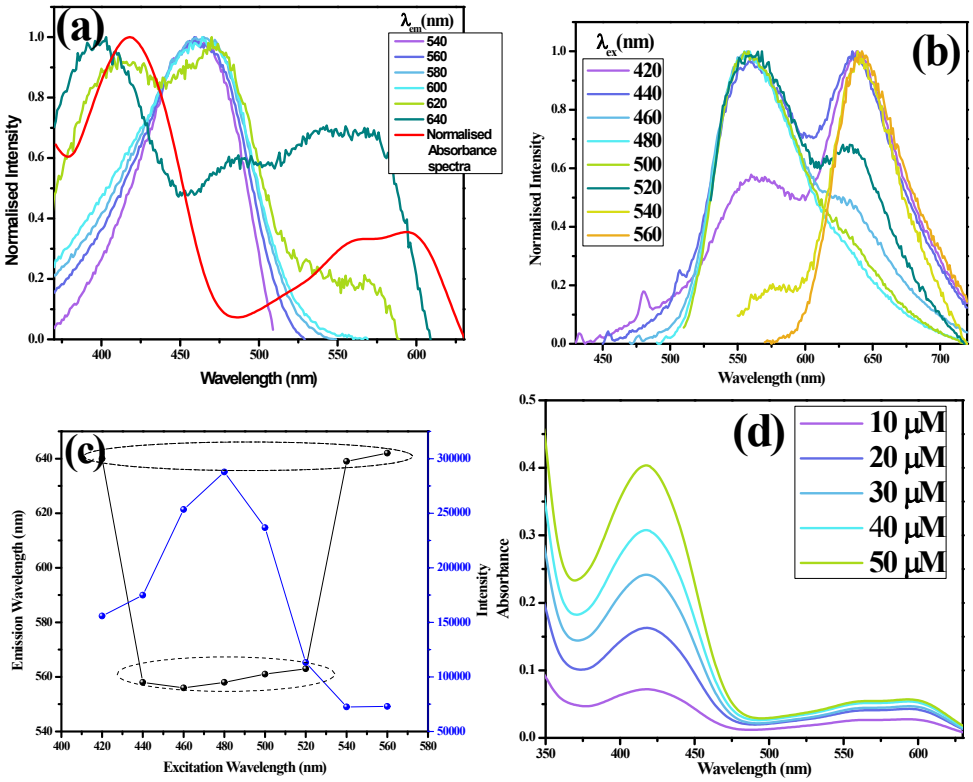

Figure S7(a). Normalised Absorption spectra; Normalised Excitation spectra with varying λ_{em} **(b)** Emission spectra with varying λ_{ex} and **(c)** Scatter plot for representing emission wavelength at maximum Intensity at varying excitation wavelength for HCQ (10 μM) in DMSO **(d)** Absorbance spectra of HCQ with increasing concentration of HCQ in DMSO

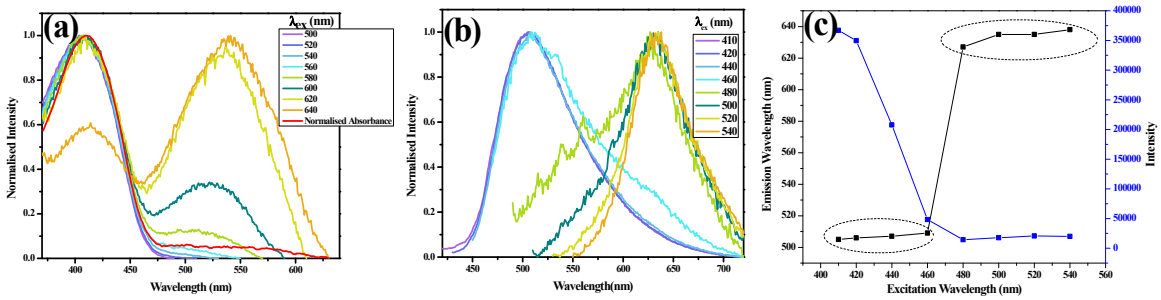

Figure S8(a). Normalised Absorption spectra; Normalised Excitation spectra with varying λ_{em} **(b)** Emission spectra with varying λ_{ex} and **(c)** Scatter plot for representing emission wavelength at maximum Intensity at varying excitation wavelength for HCQ (10 μM) in CH_3CN.

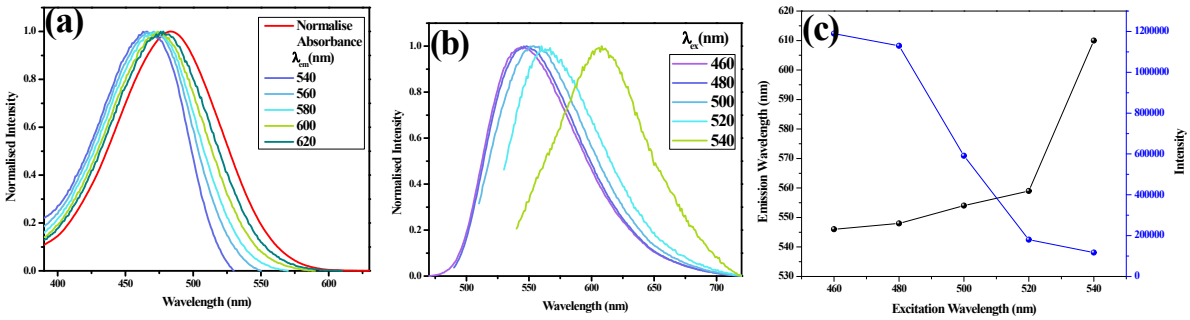

Figure S9(a). Normalised Absorption spectra; Normalised Excitation spectra with varying λ_{em} **(b)** Emission spectra with varying λ_{ex} and **(c)** Scatter plot for representing emission wavelength at maximum Intensity at varying excitation wavelength for HCQ (10 μM) in MeOH.

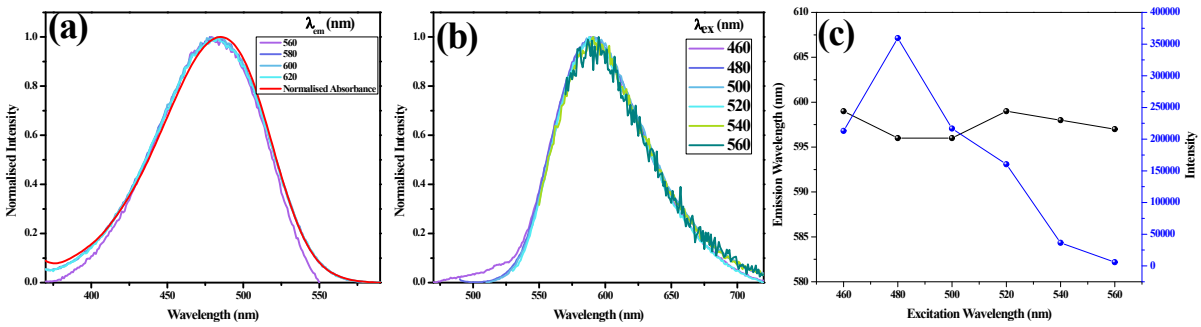

Figure S10(a). Normalised Absorption spectra; Normalised Excitation spectra with varying λ_{em} **(b)** Emission spectra with varying λ_{ex} and **(c)** Scatter plot for representing emission wavelength at maximum Intensity at varying excitation wavelength for HCQ (10 μM) in Water.

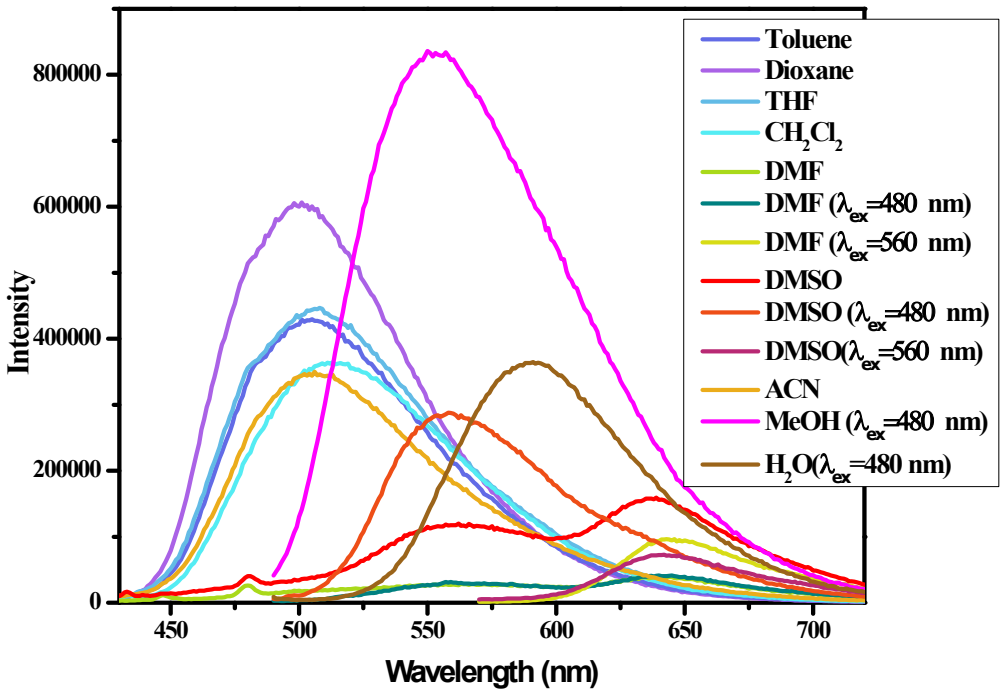

Figure S11. Emission spectra of HCQ (10 μM) in different solvents with increasing $E_T(30)$/kcal mol^{-1}; λ_{ex}=420 nm unless specified.

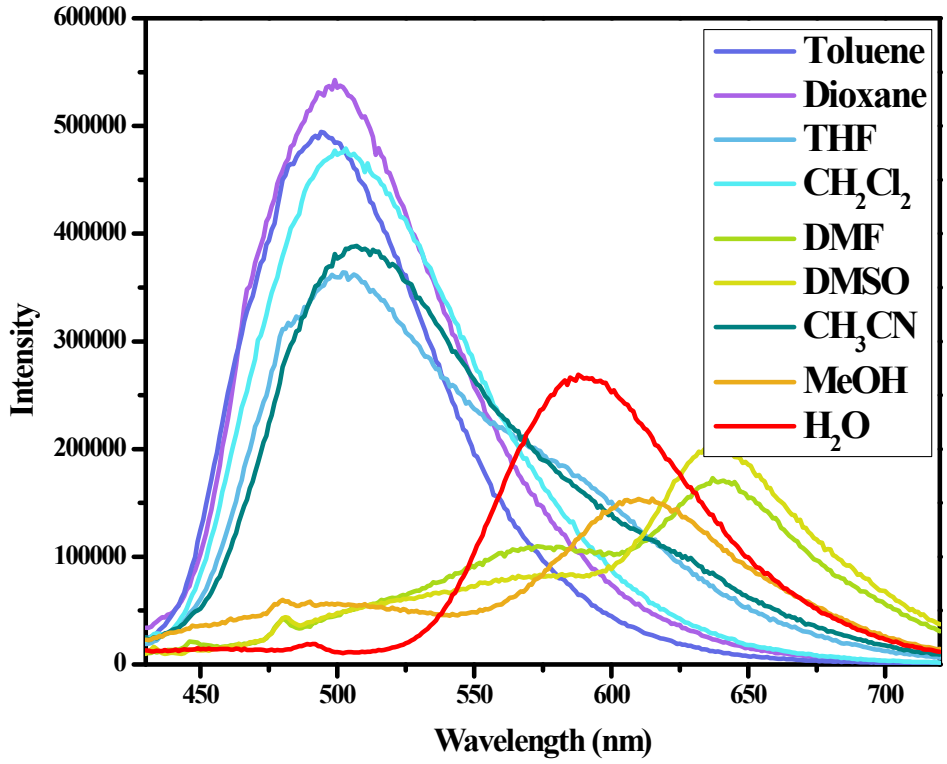

Figure S12. Emission spectra of HCQ (10 μM) in the presence of TFA (100 μM) in different solvents with increasing E_T (30)/kcal mol^{-1}; λ_{ex}=420 nm.

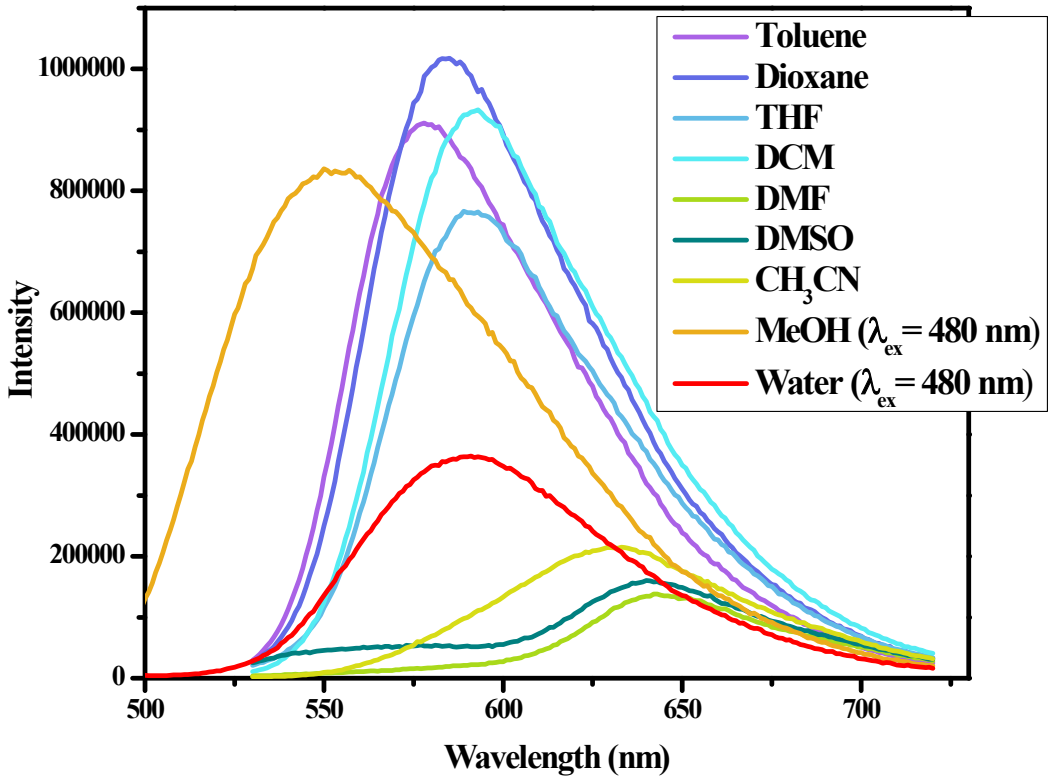

Figure S13. Emission spectra of HCQ (10 μM) in presence of TEA (100 μM) in different solvents with increasing E_T (30)/kcal mol^{-1}; λ_{ex}=520 nm.

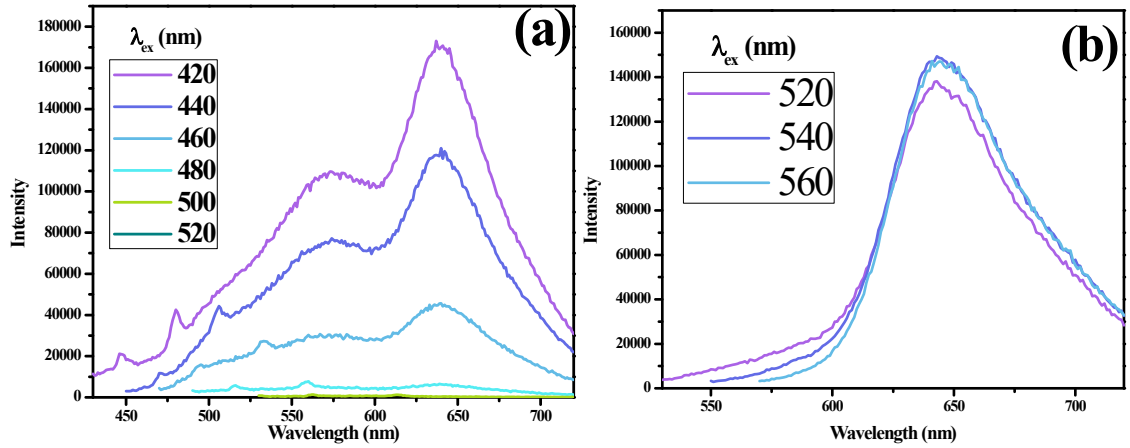

Figure S14. Emission spectra of HCQ (10 μM) in presence of **(a)** TFA (100 μM) and **(b)** TEA (100 μM) in in DMF with increasing λ_{ex}.

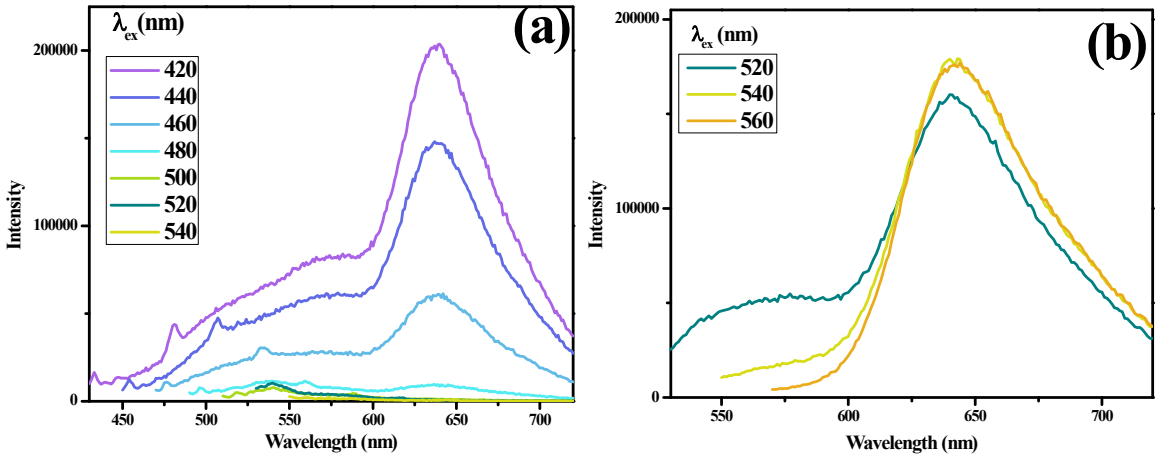

Figure S15. Emission spectra of HCQ (10 μM) in presence of **(a)** TFA (100 μM) and **(b)** TEA (100 μM) in DMSO with increasing λ_{ex}.

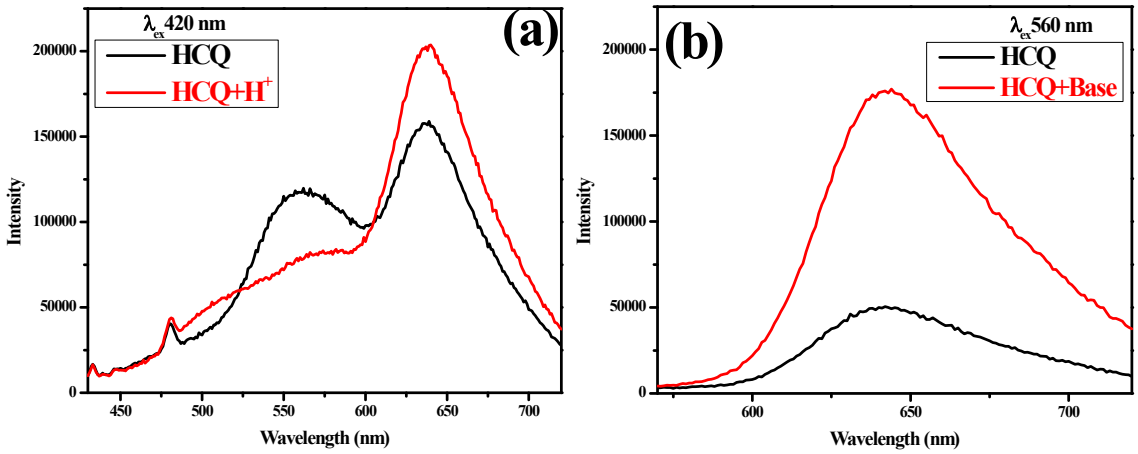

Figure S16. Emission spectra of HCQ (10 μM) in presence of **(a)** TFA (100 μM) at λ_{ex}=420 nm and **(b)** TEA (100 μM) at λ_{ex}=560 nm in DMSO.

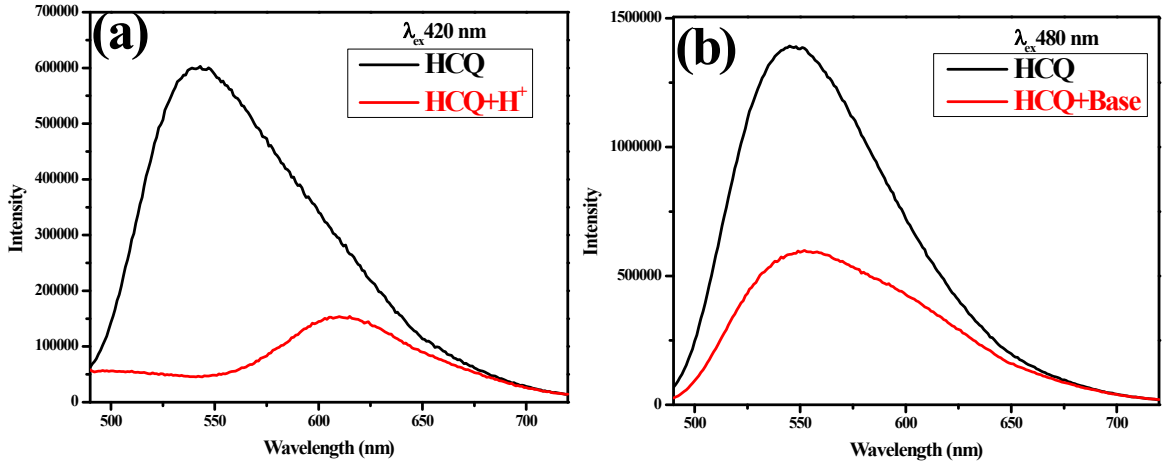

Figure S17. Emission spectra of HCQ (10 μM) in presence of **(a)** TFA (100 μM) at λ_{ex}=420 nm and **(b)** TEA (100 μM) at λ_{ex}=480 nm in MeOH.

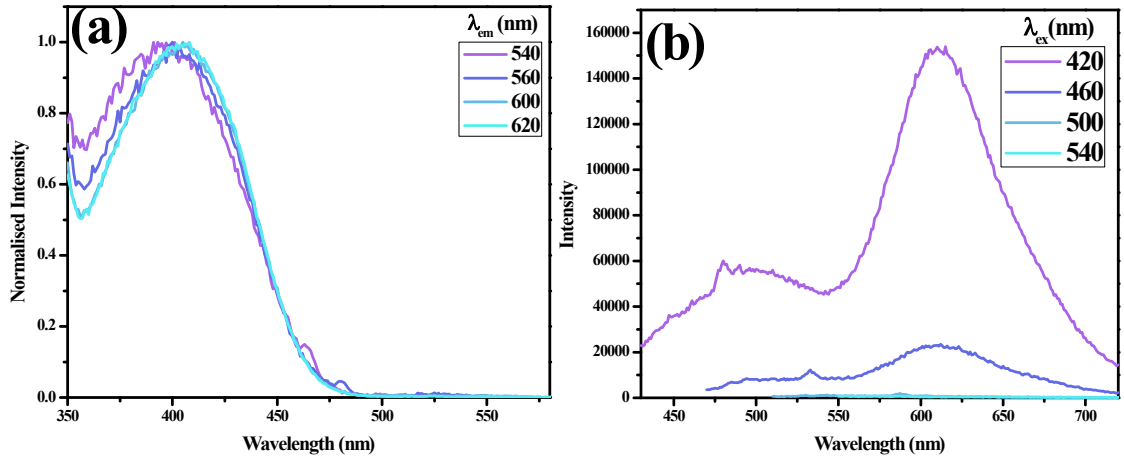

Figure S18. (a) Normalised Excitation spectra with varying λ_{em} **(b)** Emission spectra with varying λ_{ex} and for HCQ (10 μM) + TFA (100 μM) in MeOH.

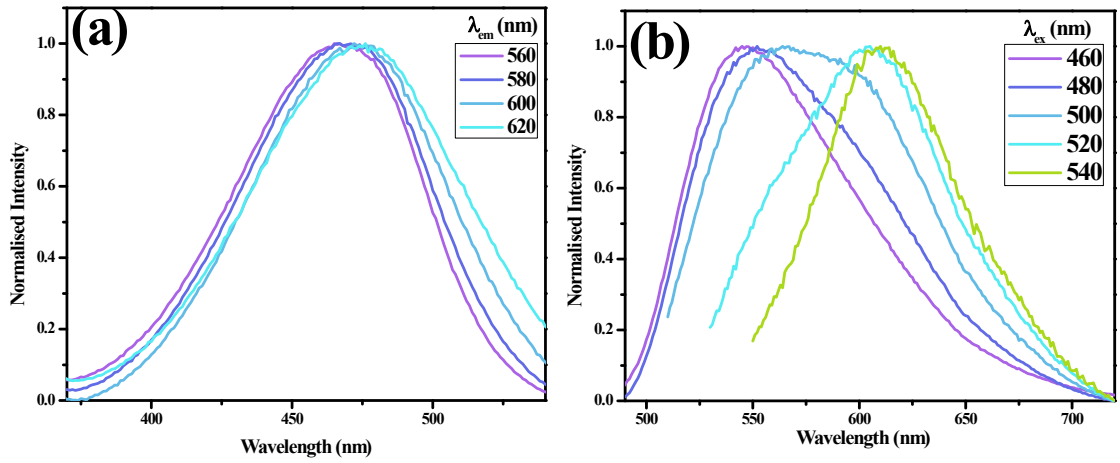

Figure S19. (a) Normalised Excitation spectra with varying λ_{em} **(b)** Emission spectra with varying λ_{ex} and for HCQ (10 μM) + TEA (100 μM) in MeOH.

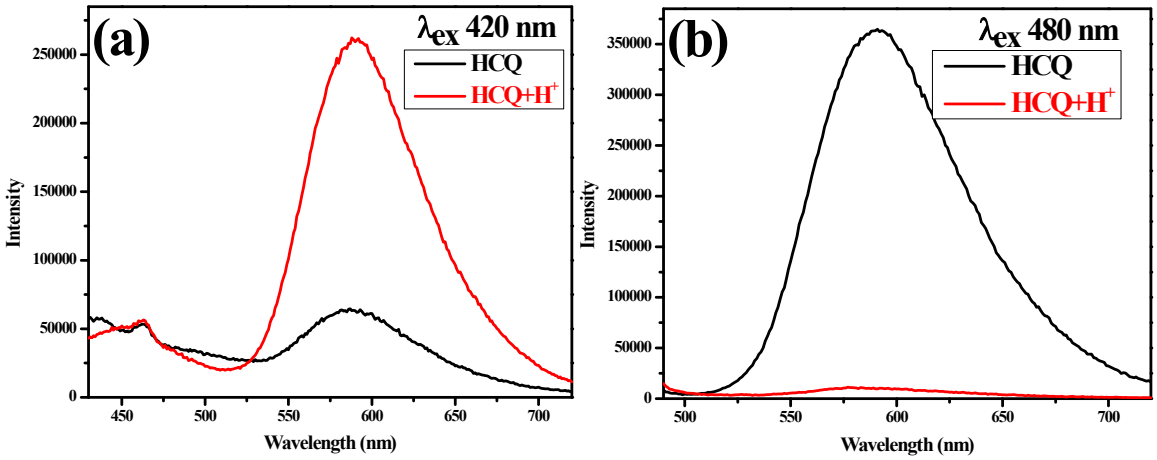

Figure S20. Emission spectra of HCQ (10 μM) in presence of **(a)** TFA (100 μM) at λ_{ex}=420 nm and **(b)** TFA (100 μM) at λ_{ex}=480 nm in Water.

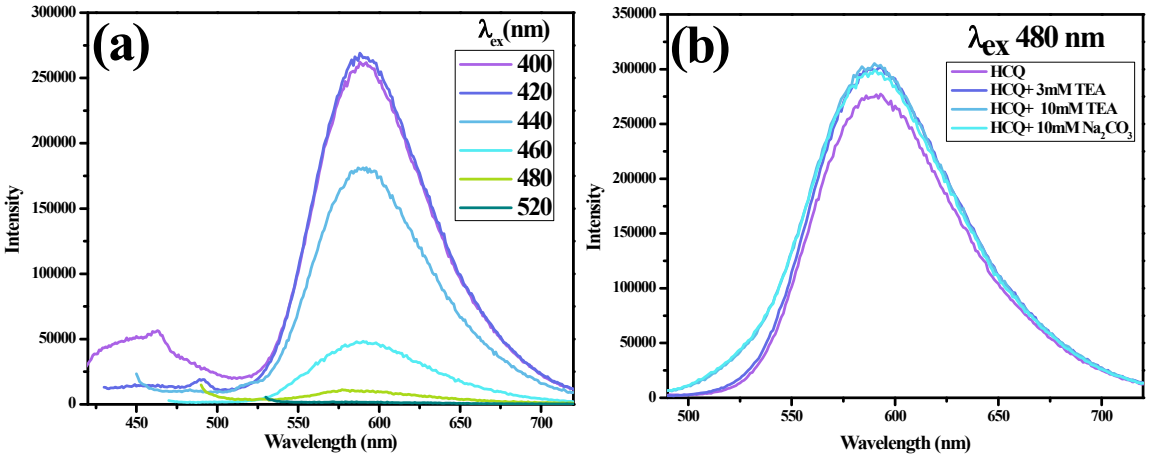

Figure S21. Emission spectra of HCQ (10 μM) in presence of **(a)** TFA (100 μM) with varying λ_{ex} **(b)** TEA and Na_2CO_3 at λ_{ex}=480 nm

Quantum yield (QY) calculation:

The fluorescence quantum yields were measured using as standards: Rhodamine 6G (Φ_R =0.94 in ethanol) and Quinine sulfate (Φ_R =0.53 in 0.1N H_2SO_4). [1]The optical density was kept below 0.15 for both sample and reference.

The quantum yield of the sample was calculated using

$\Phi_F = \Phi_R*(I/I_R)*(A_R/A)*(n^2/n_R^2)$

- Φ_F = is the quantum yield.
- I = integrated intensity for sample and I_R= integrated intensity for Reference used.
- A_R and A represent optical density for reference and sample.
- n and n_R is the refractive index of sample and reference respectively.

TCSPC Measurements:

Fluorescence decay measurements were conducted utilizing time-correlated single-photon counting. The experiments included measurements using three NanoLED at wavelengths of 405 nm. 440 nm and 510 nm. The fluorescence signals exhibited a peak of 10,000 counts. Fluorescence signals, at a specific wavelength (λ_{em}), were recorded at a magic angle of 54.7º polarization utilizing the Picosecond Photon Detection Module (PPD-850). The instrument response function (IRF) for all setups was determined using a Ludox solution. Decays were documented across wavelengths ranging from 500 to 650 nm based on sample's emission wavelength.

Decay analysis was carried out by using the EzTime decay analysis software. Analysis of the fluorescence decays employed a mono-exponential, bi-exponential and triexponential decay model, yielding goodness-of-fit parameters (χ^2) ranging between 0.9 and 1.2.

405 nm laser diode was used for studying normal form emission in dioxane, toluene, THF, CH_2Cl_2, and CH_3CN, along with protonated forms of HCQ in all the solvents. 440 nm laser diode was employed to study the lifetime of HCQ in DMF, DMSO (as depicted from the excitation spectra), MeOH, and water. This was done because of the distinct change in absorbance spectra for water and methanol at 480 nm and the excitation spectral difference observed in DMSO. To obtain the lifetime of pure protonated and deprotonated forms Laser diodes with 405 nm and 510 nm excitation were employed because the absorbance value for the enol form and keto form are centered around ~420 nm and ~520 nm.

Table S1. Absorbance wavelength $\lambda_{abs}/\lambda_{ex}$, Emission wavelength λ_{em}, Molar absorptivity (ε), Radiative rate constant for fluorescence k_f, Average Radiative Lifetimes τ_{avg}, Radiative rate constant for fluorescence k_f , and Rate constant determined for nonradiative deactivation k_{nr} and Fluorescence Quantum Yields ϕ_F for HCQ in different solvents.

Solvent	$\lambda_{abs}/\lambda_{ex}$ (nm)	λ_{em} (nm)	ε (L mol^{-1} cm^{-1})	τ_{avg} (ns)	$k_f^{(a)}$ (10^8 s^{-1})	$k_{nr}^{(b)}$ (10^8 s^{-1})	ϕ_F
Toluene	416	505	6975.35	0.542622	2.640	15.7881	0.1433#
Dioxane	412	501	8129.21	0.504892	0.2911	19.5150	0.0147#
THF	415	502	6850.34	0.483182	0.3518	20.3443	0.017#
CH_2Cl_2	417	503	6365.06	0.497557	1.6802	18.4179	0.0836#
DMF	419, 565(c)	643	4695.87 -	0.355117	0.3688	27.7908	0.0131*
DMSO	418	558	8078.24	0.307095	6.07629	26.4869	0.1866#
	567(d)	640	-	1.32848	0.3071	7.22028	0.0408*
CH_3CN	412	506	6799.24	0.470105	0.2510	21.0208	0.0118#
MeOH	483	550	9190.2	1.63835	1.6840	4.41969	0.2759*
Water	485	597	7070.16	0.739173	2.7977	10.7309	0.2068*

(a) $K_f = \Phi_F/\tau$; (b) $K_{nr} = (1 - \Phi_F)/\tau$ (c)(d) Molar absorptivity for red shifted band was not determined since only blue shifted band is concentration dependent. *Rhodamine 6G was used as Reference Standard. # Quinine Sulphate was used as Reference standard.

Table S2. The average lifetime components (τ) and their relative amplitudes(A) for HCQ (10 μM) at specified λ_{em} in different solvents recorded using 405nm Laser Diode.

Solvent	Emission wavelength (nm)	Average lifetime (ns)	χ^2	τ_1(ns)	A1(%)	τ_2(ns)	A2 (%)	τ_3(ns)	A3 (%)
Toluene	505	0.542622	1.19	0.542622	100%	-	-	-	-
	578	0.616306	1.05	0.57899	91.12%	1.81985	8.88%	-	-
Dioxane	501	0.504892	1.16	0.461278	90.61%	5.77114	9.39%	-	-
	580	0.982192	1.11	0.547853	32.39%	1.44846	60.39%	7.22996	7.22%
THF	502	0.483182	1.19	0.430317	87.33%	3.1497	12.67%	-	-
	589	1.16696	1.08	1.09741	89.9%	2.67738	10.1%	-	-
CH_2Cl_2	503	0.497557	1.06	0.471366	93.0%	1.89651	7.0%	-	-
	593	0.662016	1.18	0.662016	100 %	-	-	-	-
DMF	560	0.355117	1.13	0.31993	89.53%	5.9816	10.47%	-	-
	643	1.42492	1.05	1.42492	100%	-	-	-	-
DMSO	560	0.247467	1.08	0.215881	86.68%	5.20629	13.32%	-	-
	640	1.54665	1.16	0.816442	0.32%	1.55106	99.68%	-	-
CH_3CN	506	0.470105	1.19	0.438608	92.13%	2.93994	7.87%	-	-
	630	1.0418	1.03	0.793598	54.32%	1.65887	45.68%	-	-

χ^2=Goodness of fit parameter

Table S3. The average lifetime components (τ) and their relative amplitudes(A) for HCQ (10 μM) at specified λ_{em} in different solvents recorded using 440 nm Laser Diode.

Solvent	Emission wavelength (nm)	Average lifetime (ns)	χ^2	τ_1(ns)	A1(%)	τ_2(ns)	A2 (%)	τ_3(ns)	A3 (%)
DMF	560	0.646442	1.18	1.47391	11.7%	10.9861	49.14%	0.275248	39.16%
	643	1.48556	1.03	1.40204	93.34%	9.03655	6.66%	-	-
DMSO	560	0.307095	1.00	1.54159	10.9%	12.0639	25.62%	0.200582	63.47%
	640	1.32848	1.19	0.104494	1.66%	1.60851	95.04%	11.303	3.3%
MeOH	550	1.63835	1.19	3.65826	18.33%	10.7473	36.61%	0.856391	45.06%
	610	0.827696	1.16	0.46748	9.4%	0.840508	83.99%	8.38423	6.61%
Water	597	0.739173	1.06	0.739173	100%	-	-	-	-

Note: The Lifetime Data for DMSO and DMF was determined using both 405 nm and 440 nm Laser diode due to the difference in their absorbance and excitation spectra.

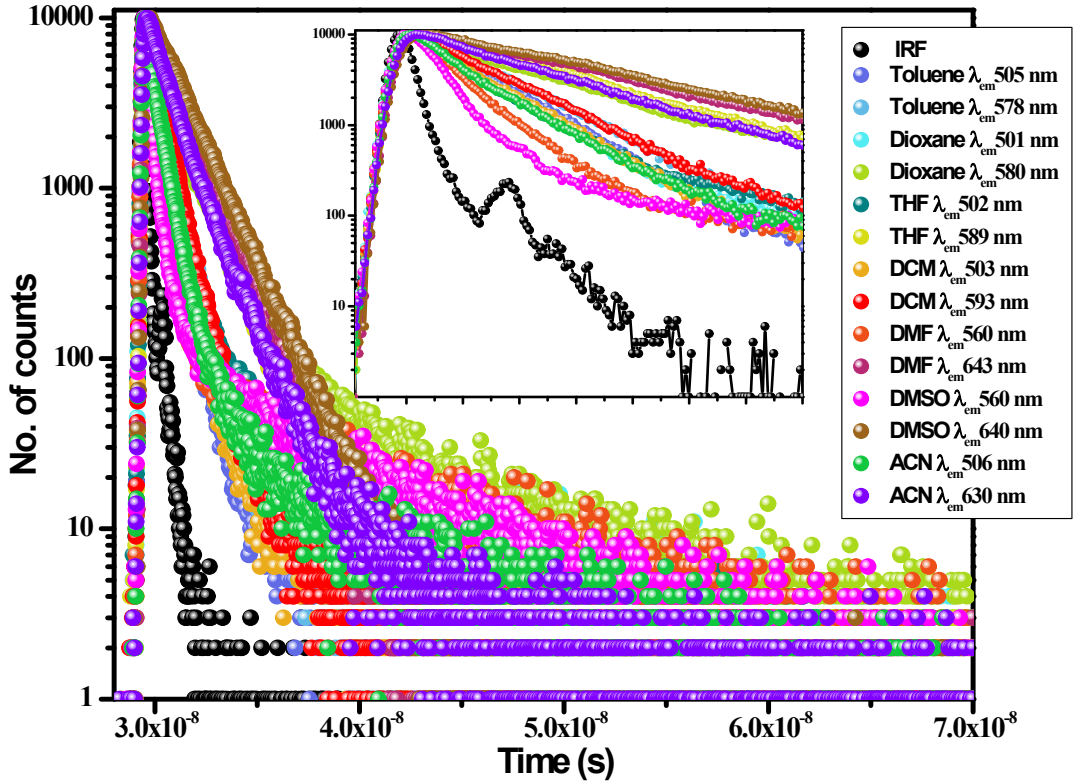

Figure S22. Fluorescence intensity decays for HCQ (10 μM) at specified λ_{em} in different solvents recorded using 405 nm Laser Diode.

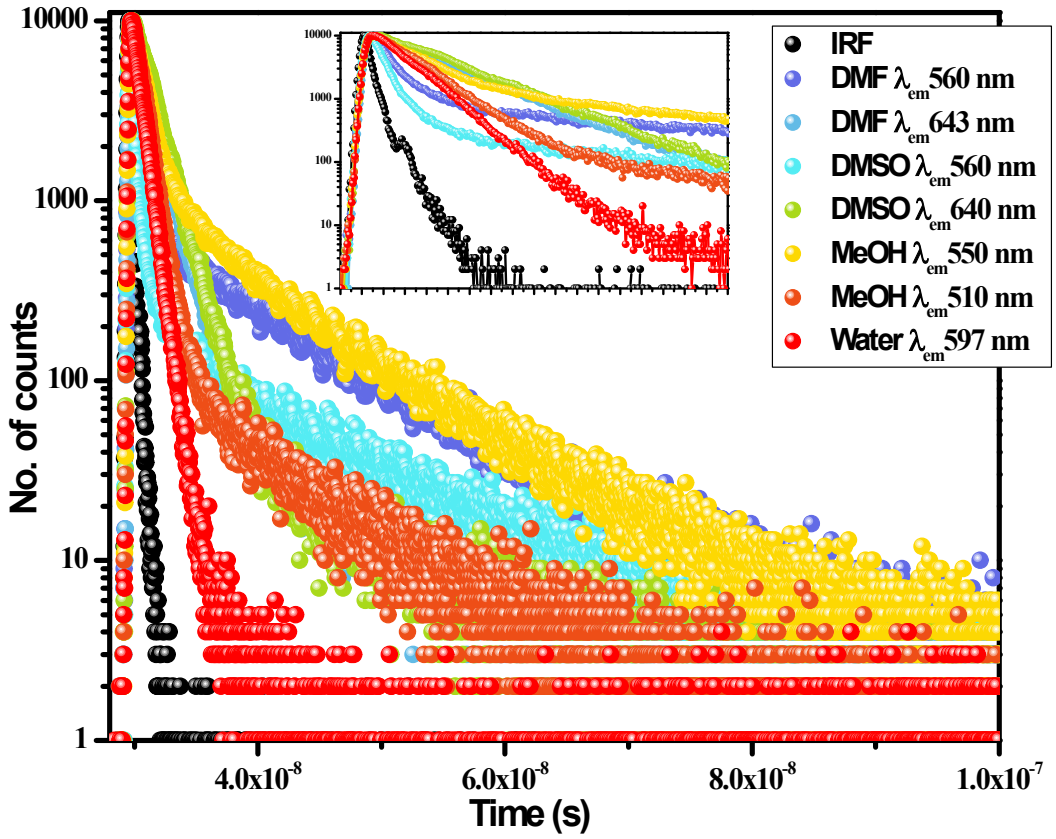

Figure S23. Fluorescence intensity decays for HCQ (10 μM) at specified λ_{em} in different solvents recorded using 440 nm Laser Diode.

Table S4. The average lifetime components (τ) and their relative amplitudes(A) for HCQ (10 μM) with TFA (100 μM) at specified λ_{em} in different solvents recorded using 405 nm Laser Diode.

Solvent	Emission wavelength (nm)	Average lifetime (ns)	χ^2	τ_1(ns)	A1(%)	τ_2(ns)	A2 (%)
Toluene	501	0.552895	1.14	0.552895	100%	-	-
Dioxane	500	0.439086	1.01	0.417861	93.85%	1.95729	6.15%
THF	502	0.48413	1.12	0.417821	83.55%	2.49936	16.45%
CH_2Cl_2	503	0.437324	1.05	0.419131	94.91%	2.30037	5.09%
DMF	560	0.349951	1.20	0.316207	89.75%	5.33899	10.25%
	643	1.4007	0.99	0.741843	2.28%	1.43029	97.72%
DMSO	560	0.230704	1.16	0.213816	92.29%	4.269	7.71%
	640	1.53993	1.07	1.53993	100%	-	-
CH_3CN	507	0.485965	1.16	0.438568	88.36%	2.71022	11.64%
MeOH	610	0.842419	1.19	0.842419	100.0%	-	-
Water	597	0.74185	1.12	0.74185	100%	-	-

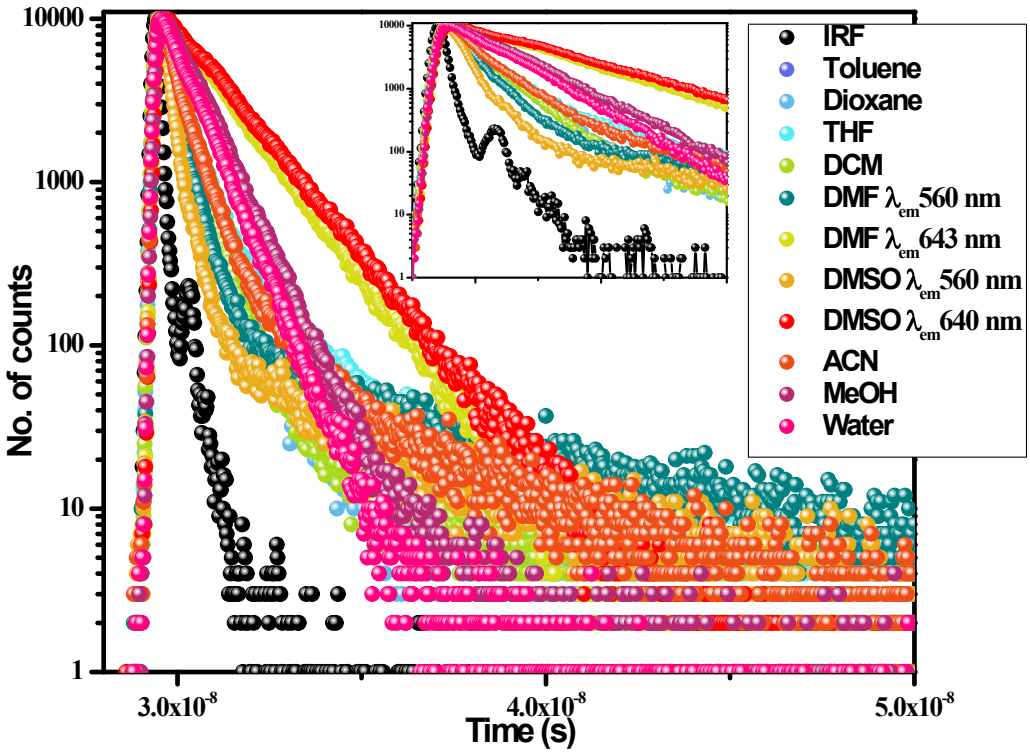

Figure S24. Fluorescence intensity decays for HCQ (10 μM) with TFA (100 μM) at specified λ_{em} in different solvents recorded using 405 nm Laser Diode.

Table S5. The average lifetime components (τ) and their relative amplitudes(A) for HCQ (10 μM) with TEA (100 μM) at specified λ_{em} in different solvents recorded using 510 nm Laser Diode.

Solvent	Emission wavelength (nm)	Average lifetime (ns)	χ^2	τ_1(ns)	A1(%)	τ_2(ns)	A2 (%)
Toluene	578	2.50547	1.009	2.50547	100%	-	
Dioxane	580	2.47924	1.06	2.47924	100%	-	-
THF	589	2.10209	1.21	1.88524	87.39%	10.3675	12.61%
CH_2Cl_2	593	2.62595	1.18	2.62595	100%	-	-
DMF	640	1.46116	1.11	1.46116	100%	-	-
DMSO	640	1.61908	1.11	1.61908	100%	-	-
CH_3CN	630	1.69918	1.69	1.69918	100.0%	-	-
Water	597	0.749221	1.20	0.749221	100%	-	-

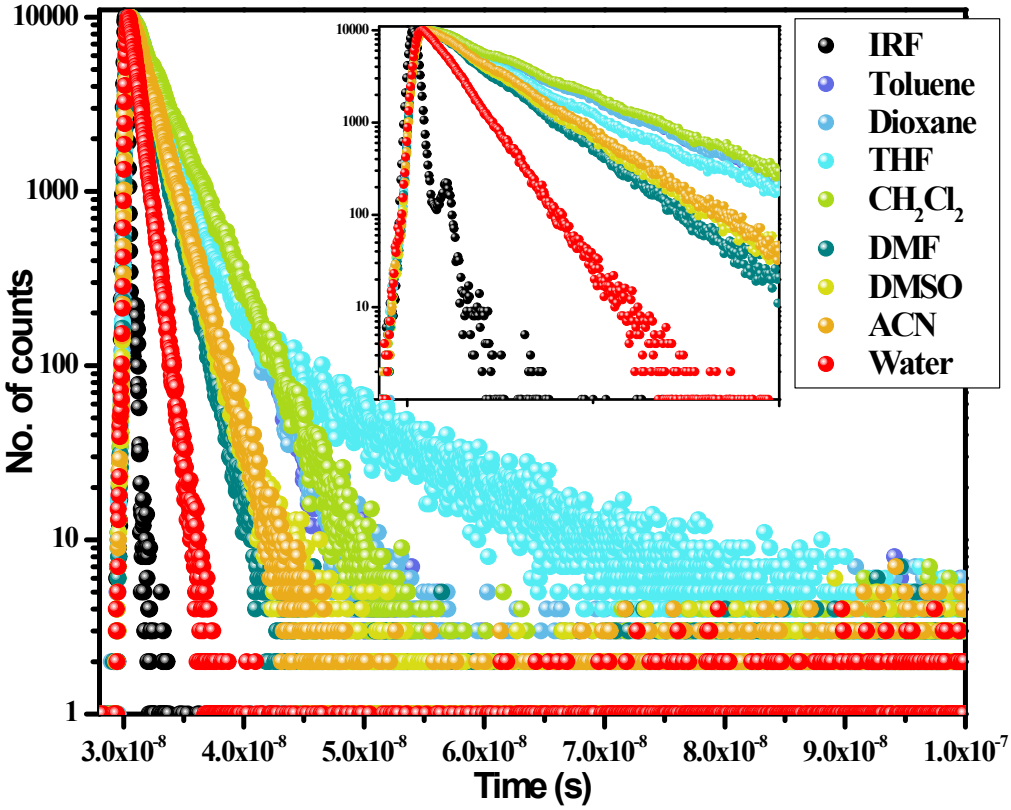

Figure S25. Fluorescence intensity decays for HCQ (10 μM) with TEA (100 μM) at specified λ_{em} in different solvents recorded using 510 nm Laser Diode.

Karl Fischer Measurements and Sample preparation:

Sample Preparation for Karl Fischer measurements was carried out by weighing 0.5 ml of dry solvent from the solvent bottle. All the measurements were carried out at room temperature.

- Titre mode was used to standardize the KF instrument. The KF values obtained for all the standardization procedures were in the range of 4 to 5.
- Blank mode was then used to determine the blank solvent moisture content.
- Using Sample mode, the moisture content was measured by addition of known percentage of water to the dry solvents and tabulated alongside the values as added for conducting the fluorescence and UV spectroscopy measurements.
- Similarly for unknown samples the moisture was determined and compared to the data obtained using fluorescence and UV from ratio of I/I_o and A/A_o respectively.
- The formula stored in the memory to find moisture is given below:

$$\% \, Moisture = \frac{\textbf{Ep ml x KF Titre value (mg/ml)}}{\textbf{Sample Wt. (gms) x 10}}$$

Where,

EP ml= End point in ml

Sample Wt. = Weight of sample taken in grams

KF Titre Value= Titre value of KF in mg/ml.

Water Detection:

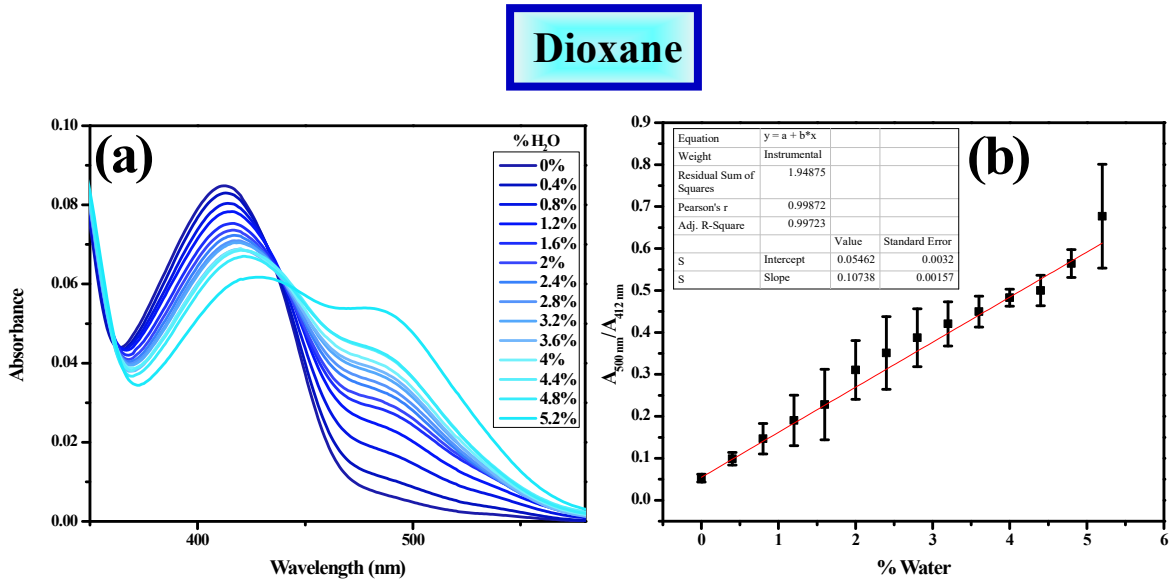

Figure. S26 (a) Fluorescence emission spectra **(b)** Scatter plot at A_{500}/A_{412} for HCQ(10 μM) with increasing percentage of water(0-5.2%) in Dioxane.

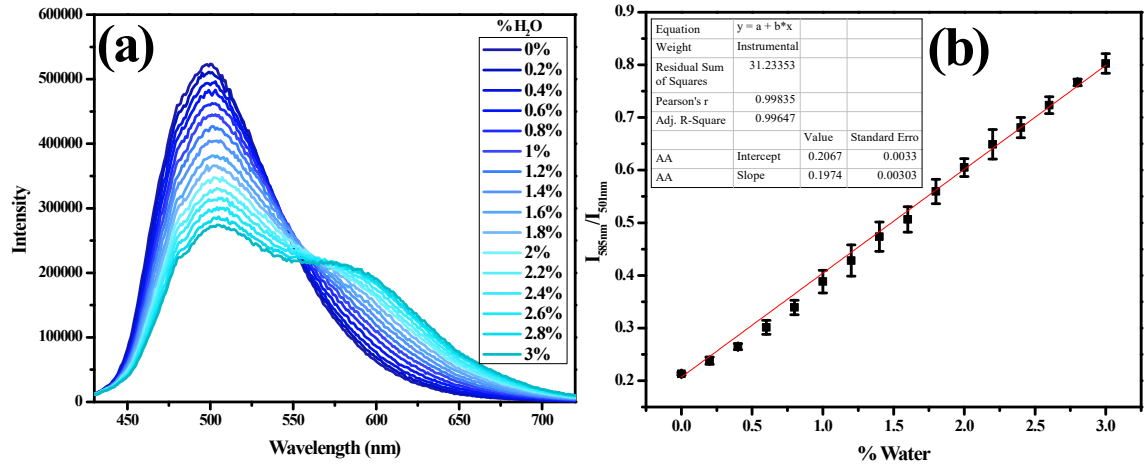

Figure S27. (a) Fluorescence emission spectra **(b)** Scatter plot at I_{580}/I_{500} for HCQ (10 μM)+TFA (100 μM) with increasing percentage of water(0-3%) in Dioxane.

Table S6. Tabular column depicting titration of water with HCQ using (10 μM) Fluorescence (at I_{580}/I_{500}), Absorbance(A_{500}/A_{412}) and Karl Fischer (without HCQ) in Dioxane.

% H_2O	I_{580}/I_{500} for Dioxane	% H_2O	A_{500}/A_{412} for Dioxane	% moisture from Karl Fischer Instrument
0	0.2129 (± 0.0025)	0	0.0527 (± 0.0093)	0.0150 (0%)
0.2	0.2381 (± 0.0070)	0.4	0.0987 (± 0.0150)	
0.4	0.2646 (± 0.0055)	0.8	0.1468 (± 0.0364)	
0.6	0.3012 (± 0.0134)	1.2	0.1901 (± 0.0603)	0.9523 (1%)
0.8	0.3391 (± 0.0137)	1.6	0.2281 (± 0.0839)	
1	0.3882 (± 0.0215)	2	0.3105 (± 0.0698)	
1.2	0.4281 (± 0.0296)	2.4	0.3510 (± 0.0867)	1.8330 (2%)
1.4	0.4734 (± 0.0277)	2.8	0.3872 (± 0.0691)	
1.6	0.5063 (± 0.0239)	3.2	0.4205 (± 0.0526)	
1.8	0.5595 (± 0.0231)	3.6	0.4496 (± 0.0367)	2.8578 (3%)
2	0.6050 (± 0.0169)	4	0.4830 (± 0.0201)	
2.2	0.6490 (± 0.0281)	4.4	0.4997 (± 0.0362)	
2.4	0.6808 (± 0.0193)	4.8	0.5645 (± 0.0332)	4.0451 (4%)
2.6	0.7234 (± 0.0159)	5.2	0.6770 (± 0.1238)	
2.8	0.7667 (± 0.0062)	-		
3	0.8027 (± 0.0188)	-		4.9098 (5%)

<u>Determination of % water for unknown sample in Dioxane:</u>

I_{580}= 188250, I_{500}= 320510

I_{580}/I_{500} = 0.5873--------1.8-2% from Fluorescence spectroscopy

A_{500} = 0.03698 A_{412} = 0.05256

A_{500}/A_{412} = 0.7035---------->5.2% from UV spectroscopy

Percentage moisture detected using Karl Fischer: 1.5946%

THF

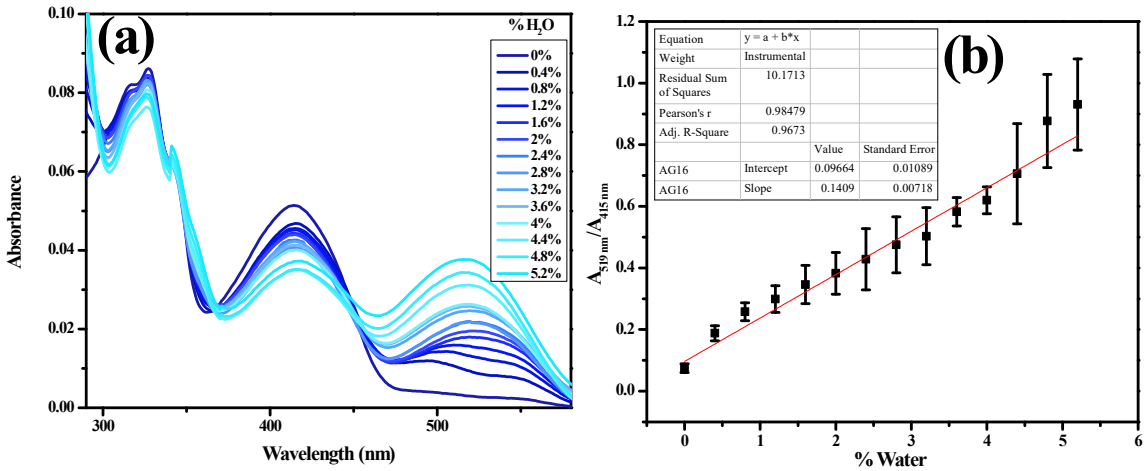

Figure S28. (a) Fluorescence emission spectra **(b)** Scatter plot at A_{500}/A_{412} for HCQ (10 μM) with increasing percentage of water (0-5.2%) in THF.

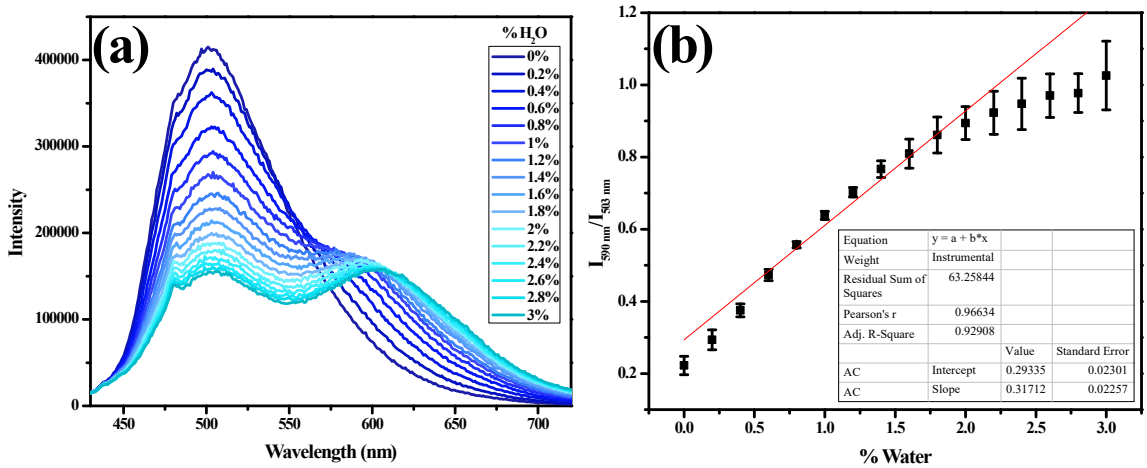

Figure S29. (a) Fluorescence emission spectra **(b)** Scatter plot at I_{580}/I_{500} for HCQ (10 μM) +TFA (100 μM) with increasing percentage of water (0-3%) in THF.

Table S7. Tabular column depicting titration of water with HCQ using (10 μM) Fluorescence (at I_{590}/I_{503}) , Absorbance(A_{519}/A_{415}) and Karl Fischer (without HCQ) in THF.

% H_2O	I_{590}/I_{503} for THF	% H_2O	A_{519}/A_{415} for THF	Standard Deviation	% moisture from Karl Fischer Instrument
0	0.2222 (± 0.0256)	0	0.0744 (± 0.0143)		0.1150
0.2	0.2934 (± 0.0275)	0.4	0.1879 (± 0.0246)		
0.4	0.3752 (± 0.0178)	0.8	0.2577 (± 0.0293)		
0.6	0.4730 (± 0.0154)	1.2	0.2990 (± 0.0433)		1.1732(1%)
0.8	0.5567 (± 0.0087)	1.6	0.3461 (± 0.0623)		
1	0.6382 (± 0.0112)	2	0.3825 (± 0.0678)		
1.2	0.7026 (± 0.0132)	2.4	0.4280 (± 0.0995)		2.1030 (2%)
1.4	0.7665 (± 0.0231)	2.8	0.4749 (± 0.0910)		
1.6	0.8096 (± 0.0402)	3.2	0.5031 (± 0.0926)		
1.8	0.8612 (± 0.0499)	3.6	0.5822 (± 0.0463)		3.1660 (3%)
2	0.8942 (± 0.0459)	4	0.6196 (± 0.0436)		
2.2	0.9228 (± 0.0596)	4.4	0.7057 (± 0.1625)		
2.4	0.9475 (± 0.0713)	4.8	0.8766 (± 0.1512)		4.1635 (4%)
2.6	0.9703 (± 0.0604)	5.2	0.9307 (± 0.1481)		
2.8	0.9773 (± 0.0536)	-	-	-	
3	1.0259 (± 0.0952)	-	-	-	5.2034 (5%)

<u>Determination of % water for unknown sample in THF:</u>

I_{590}= 207060**, I_{503}**= 299410

I_{590}/I_{503} = 0.6915--------**1-1.2%** from Fluorescence spectroscopy

A_{519} =0.01702 **A_{415}** = 0.07129

A_{519}/A_{415} =0.2387 ----------**0.4-0.8**% from UV spectroscopy

Percentage moisture detected using Karl Fischer: 1.4348%

DMSO

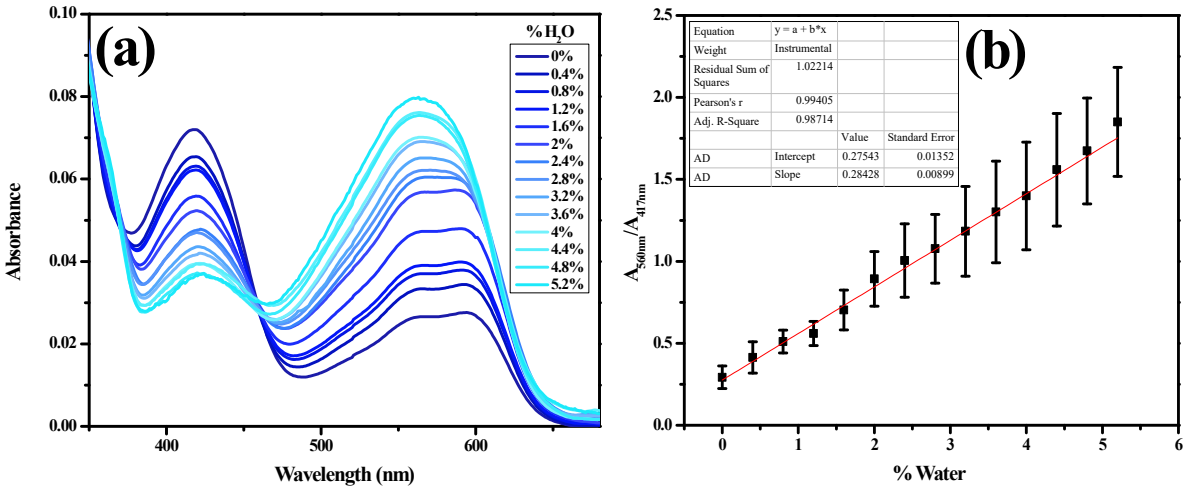

Figure S30. (a) Fluorescence emission spectra **(b)** Scatter plot at A_{560nm}/A_{417nm} for HCQ (10 μM) with increasing percentage of water (0-5.2%) in DMSO.

Table S8. Tabular column depicting titration of water with HCQ using (10 μM), Absorbance(A_{560nm}/A_{417nm}) and Karl Fischer (without HCQ) in DMSO.

% H_2O	A_{560nm}/A_{417nm} for DMSO	Standard Deviation	% moisture from Karl Fischer Instrument
0	0.2928 (± 0.0685)		0.0644
0.4	0.4137 (± 0.0957)		
0.8	0.5107 (± 0.0698)		
1.2	0.5598 (± 0.0738)		0.9445 (1%)
1.6	0.7032 (± 0.1217)		
2	0.8931 (± 0.1662)		1.8418 (2%)
2.4	1.0052 (± 0.2236)		
2.8	1.0769 (± 0.2093)		
3.2	1.1832 (± 0.2739)		2.7368 (3%)
3.6	1.3007 (± 0.3100)		
4	1.3990 (± 0.3286)		3.4229 (4%)
4.4	1.5586 (± 0.3436)		
4.8	1.6734 (± 0.3229)		
5.2	1.8506 (± 0.3319)		4.2867 (5%)

Determination of % water for unknown sample in DMSO:

A_{560nm} =0.0442733, A_{417nm} = 0.0576709

A_{560nm}/A_{417nm} =0.76768----------1.6-2% from UV spectroscopy

Percentage moisture detected using Karl Fischer: 2.2800%

CH_3CN

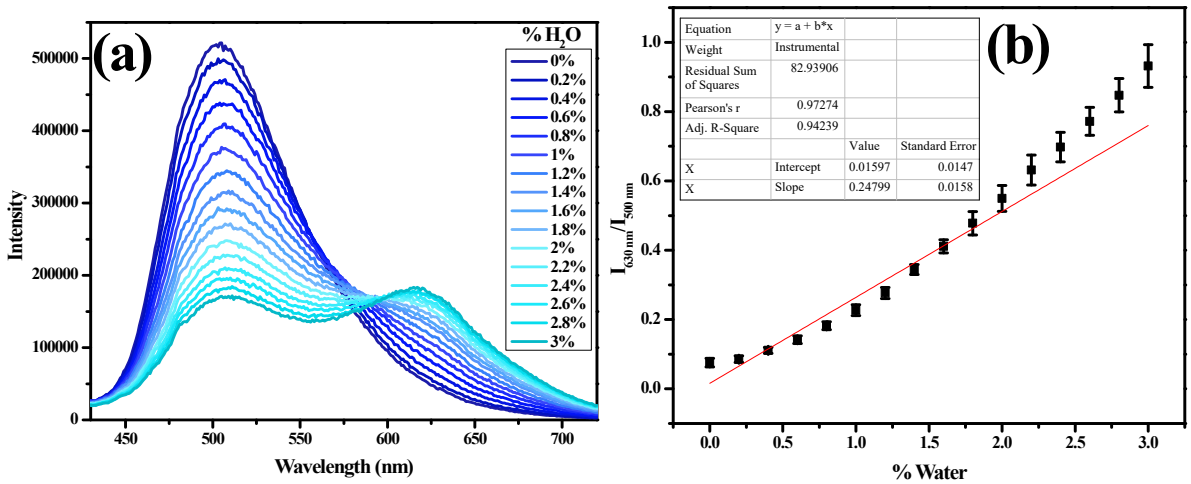

Figure S31. (a) Fluorescence emission spectra **(b)** Scatter plot at $I_{630}/I_{500}$for HCQ (10 μM) +TFA (100 μM) with increasing percentage of water (0-3%) in CH_3CN.

Table S9. Tabular column depicting titration of water with HCQ using (10 μM), Absorbance(I_{630}/I_{500}) and Karl Fischer (without HCQ) in CH_3CN.

% H_2O	I_{630}/I_{500} for CH_3CN	% moisture from Karl Fischer Instrument
0	0.0756 (± 0.0127)	(0.0894)
0.2	0.0856 (± 0.0095)	
0.4	0.1110 (± 0.0082)	
0.6	0.1419 (± 0.0111)	
0.8	0.1819 (± 0.0113)	1.0732(1%)
1	0.2269 (±0.0158)	
1.2	0.2765 (± 0.0158)	
1.4	0.3444 (± 0.0142)	
1.6	0.4111 (± 0.0193)	1.9304(2%)
1.8	0.4778 (± 0.0337)	
2	0.5494 (± 0.0372)	
2.2	0.6315 (± 0.0433)	
2.4	0.6975 (± 0.0426)	3.0929(3%)
2.6	0.7718 (± 0.0405)	
2.8	0.8472 (± 0.0480)	
3	0.9316 (± 0.0610)	

Determination of % water for unknown sample in CH_3CN:

I_{630}=152030, I_{500}= 197190

I_{630}/I_{500}=2.6 % ----------from fluorescence spectroscopy

Percentage moisture detected using Karl Fischer: 2.6295%

MeOH

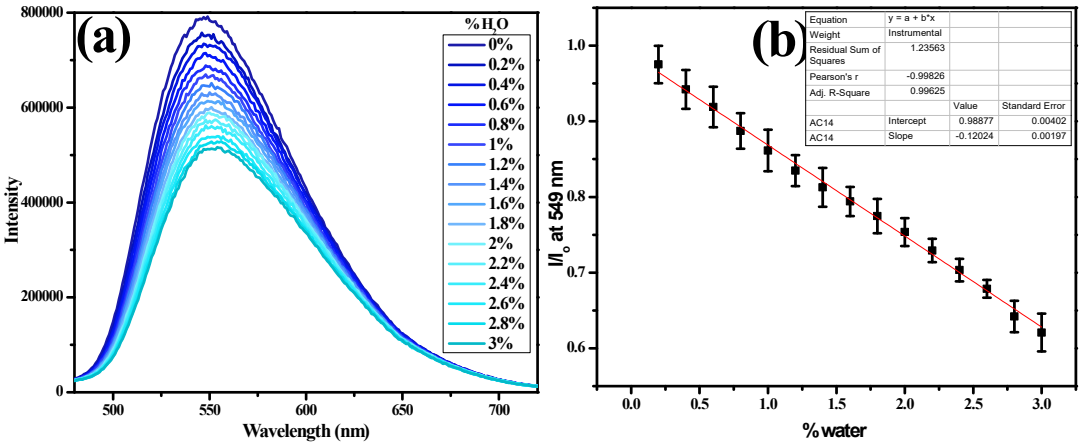

Figure S32. (a) Fluorescence emission spectra **(b)** Scatter plot at I/I_0 at 550 nm for HCQ (10 μM) with increasing percentage of water (0-3%) in MeOH.

Table S10. Tabular column depicting titration of water with HCQ using (10 μM), Fluorescence(I/I_0) at 550 nm and Karl Fischer (without HCQ) in MeOH.

% H_2O	I/I_0 for MeOH at 549 nm	% moisture from Karl Fischer Instrument
0	1(± 0)	0.0863
0.2	0.9750 (± 0.0247)	
0.4	0.9421 (± 0.0256)	
0.6	0.9189 (± 0.0268)	
0.8	0.8872 (± 0.0234)	
1	0.8614 (± 0.0274)	1.2485(1%)
1.2	0.8348 (± 0.0204)	
1.4	0.8126 (± 0.0257)	
1.6	0.7940 (± 0.0192)	
1.8	0.7747 (± 0.0226)	
2	0.7536 (± 0.0184)	2.4013(2%)
2.2	0.7292 (± 0.0154)	
2.4	0.7033 (± 0.0148)	
2.6	0.6785 (± 0.0117)	3.4598 (3%)
2.8	0.6421 (± 0.0207)	
3	0.6208 (± 0.0250)	

<u>Determination of % water for unknown sample in MeOH:</u>

I=837730, I_0= 910530

I/I_0 at 550 nm =0.92004--------0.6% from Fluorescence spectroscopy

Percentage moisture detected using Karl Fischer: 0.4090%

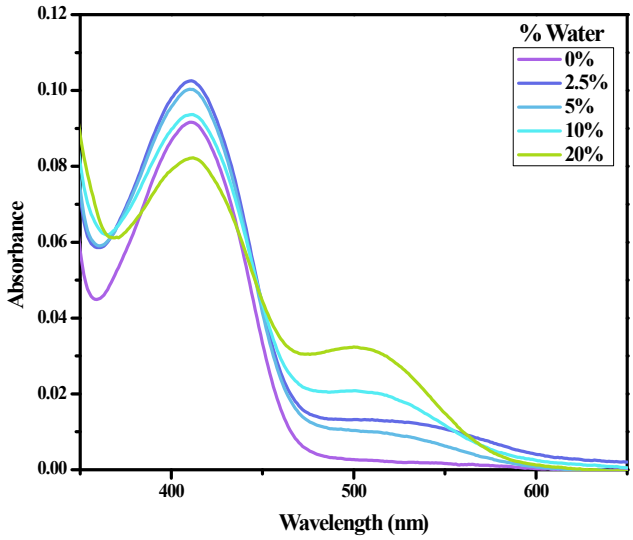

Figure S33. UV-visible spectrum for HCQ (10 μM) with increasing water concentration in CH_3CN.

Calculation of LOD and LOQ:

Limit of Detection (LOD): was calculated using the formula: LOD=3× σ/ K and Limit of Quantification (LOQ) is calculated using 10× σ/ K. Where σ is Standard Deviation of the response and K= Slope of the calibration curve

In both UV and fluorescence detection, the calibration curve was constructed by measuring the absorbance or fluorescence intensity of known concentrations of water (0-5.2% for UV and 0-3% for fluorescence) with HCQ (10 μM).

Crystal structure analysis of HCQ and ACQ:

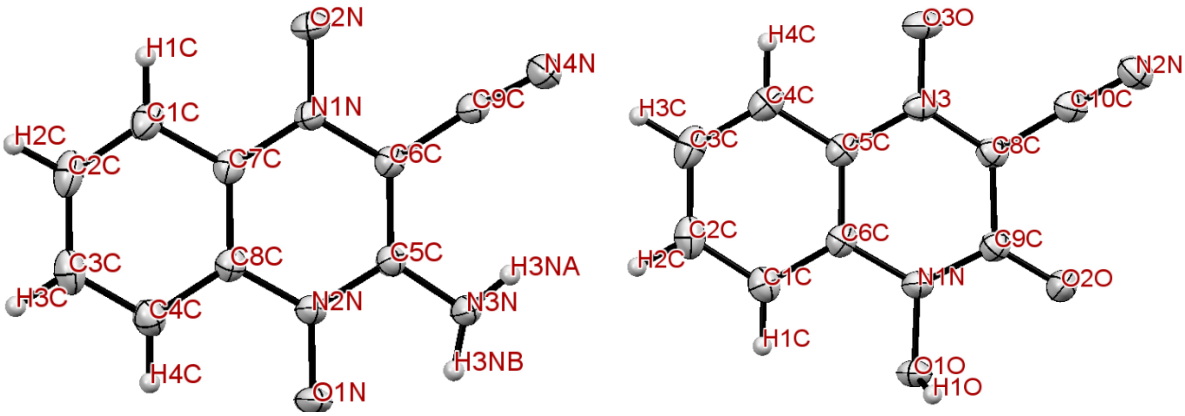

Figure S34. Labelled ORTEP structures of ACQ and HCQ

Table S11. Torsion angles for ACQ and HCQ

	Torsion Angle	Torsion (º)
ACQ	N3-C5-C6-N1	-179.94
	O1-N2-C5-C6	-179.23
	O2-N1-C6-C5	177.63
	H3NB-N3-C5-C6	-178.82
HCQ	O1-N1-C9-C8	178.43
	O3-N3-C8-C9	-179.84
	O2-C9-C8-N3	178.64
	H1-O1-N1-C9	**81.69**
	H1-O1-N1-C6	**-103.29**

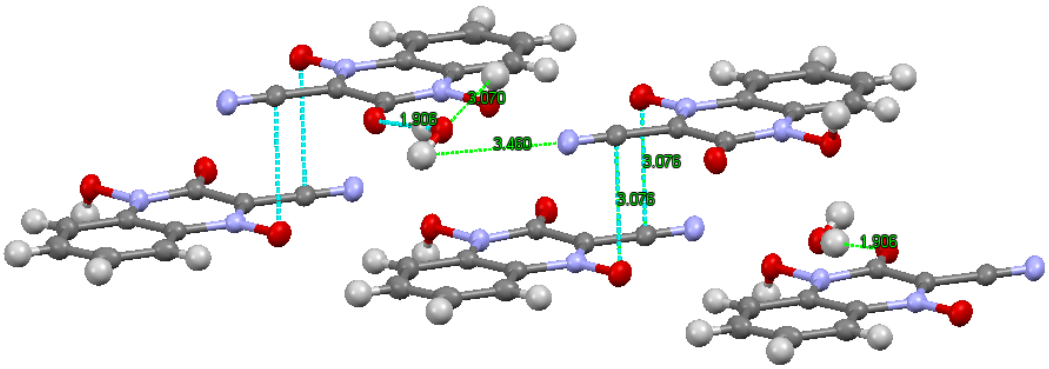

Figure S35. Crystal packing indicating water involvement of water molecule in hydrogen bonding.

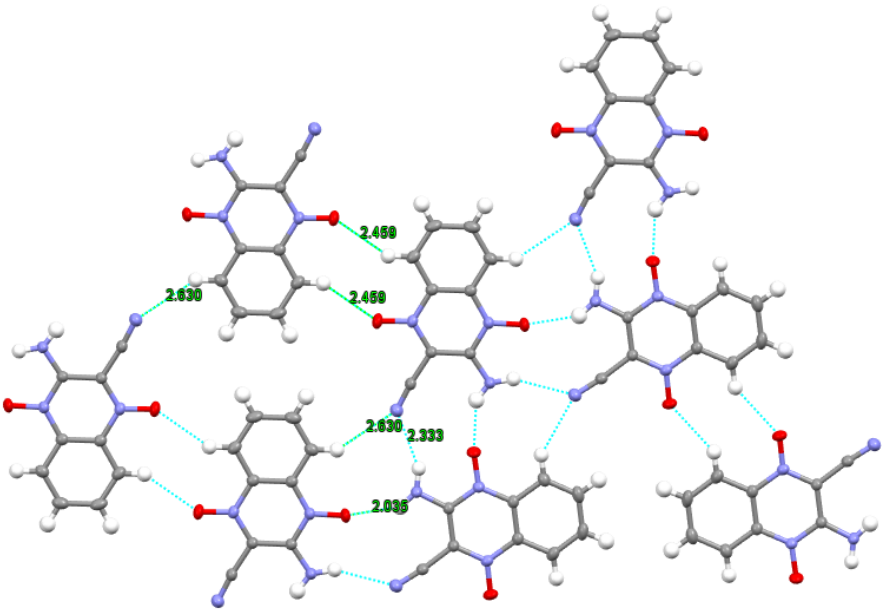

Figure S36. H-bonding in ACQ

Table S12. The S_0/S_1 transition energies, oscillator strengths of three enol (E), keto (K) and [RO$^-$---water] optimized in the S_0 electronic state, E*, K* and [RO$^-$---water] * optimized in the excited electronic state. The calculations were performed for molecule in acetonitrile using TD B3LYP/6-311+G(d,p) and solvent involved in the CPCM mode.

HCQ form	**Calculated absorbance values (S_0-S_1 transition at optimized S_0)**	**S_0-S_1 transition oscillator strength**	**Experimental absorbance values in CH_3CN**
E	428.05 nm	0.1429	412
K	523.95 nm	0.1471	532
	Calculated absorbance values (S_0-S_1 transition at optimized S_0)	**S_0-S_1 transition oscillator strength**	**Experimental absorbance values in water**
[RO$^-$---water]	505.82 nm	0.1424	480
	Calculated emission values (S_1-S_0 transition at optimized S_1)		**Experimental emission values in CH_3CN**
E*	493.69 nm	0.2163	506
K*	622.41 nm	0.1897	630
	Calculated emission values (S_1-S_0 transition at optimized S_1)	**S_1-S_0 transitions Oscillator strength**	**Experimental emission values in water**
[RO$^-$---water] *	599.66 nm	0.1907	597

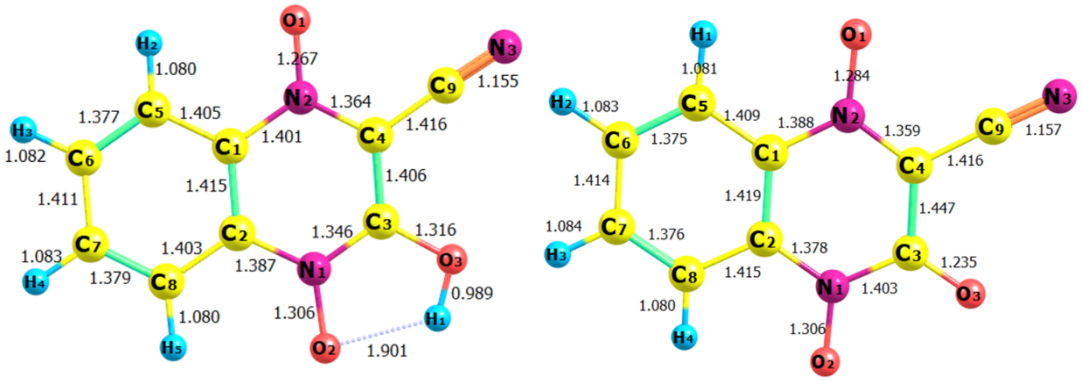

Figure S37. Ground state optimised structures of Enol and Keto forms of HCQ in acetonitrile.

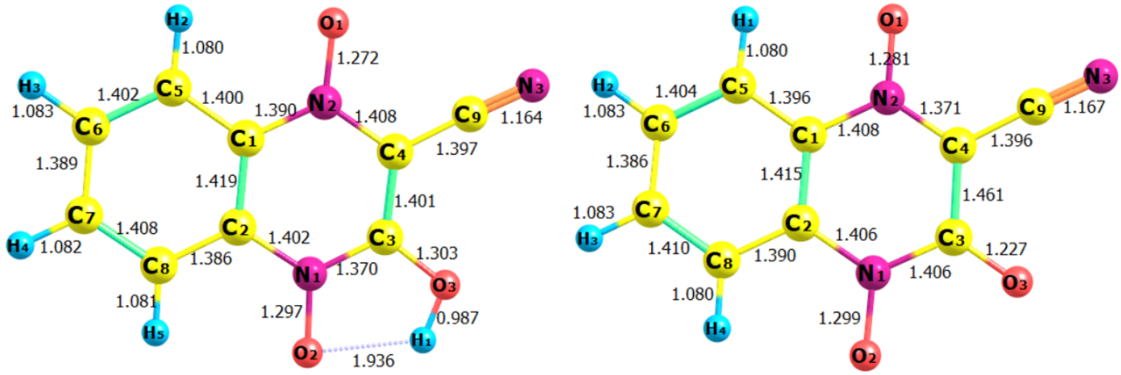

Figure S38. Excited state optimised structures of Enol and Keto forms of HCQ in acetonitrile.

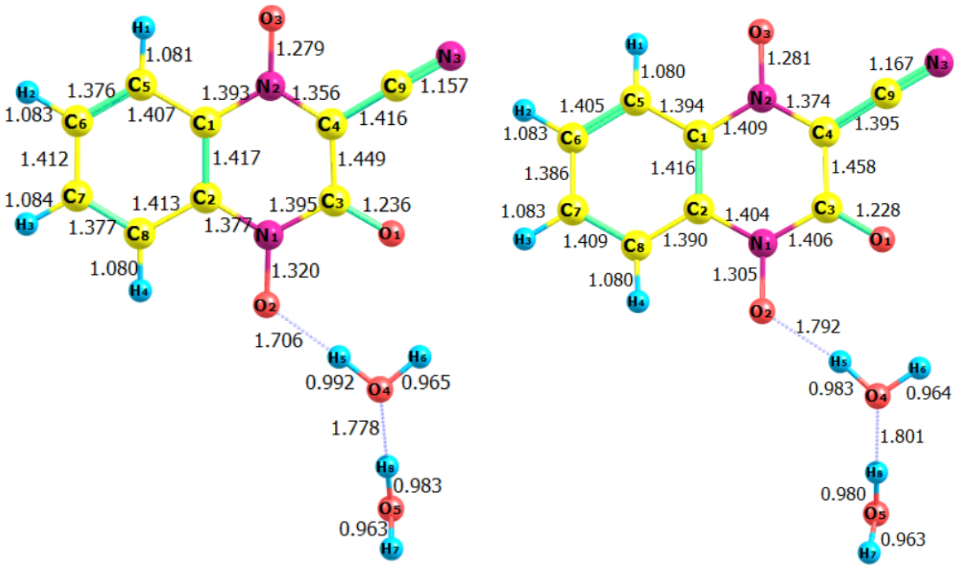

Figure S39. Ground state (left) and Excited state (right) optimised structures of [RO^{-}---water] form of HCQ in water depicting hydrogen bonding interaction.

Single Crystal Data for HCQ

exp_1386_HCQ **Deposition Number: 2270859**

Table 1 Crystal data and structure refinement for exp_1386_HCQ.

Identification code	exp_1386_HCQ
Empirical formula	$C_9H_7N_3O_4$
Formula weight	219.18
Temperature/K	93
Crystal system	monoclinic
Space group	C2/c
a/Å	16.4937(3)
b/Å	8.07760(10)
c/Å	14.6807(3)
α/°	90
β/°	107.189(2)
γ/°	90
Volume/Å^3	1868.54(6)
Z	8
ρ_{calc}g/cm^3	1.5723
μ/mm^{-1}	1.091
F(000)	915.6
Crystal size/mm^3	0.2 × 0.1 × 0.05
Radiation	Cu Kα (λ = 1.54184)
2Θ range for data collection/°	11.24 to 159.14
Index ranges	$-20 \leq h \leq 20$, $-9 \leq k \leq 5$, $-14 \leq l \leq 18$
Reflections collected	4615
Independent reflections	1954 [R_{int} = 0.0197, R_{sigma} = 0.0272]
Data/restraints/parameters	1954/0/149
Goodness-of-fit on F^2	1.037
Final R indexes [I>=2σ (I)]	R_1 = 0.0450, wR_2 = 0.1382
Final R indexes [all data]	R_1 = 0.0468, wR_2 = 0.1405
Largest diff. peak/hole / e Å^{-3}	0.64/-0.73

Table 2 Fractional Atomic Coordinates (×10^4) and Equivalent Isotropic Displacement Parameters (Å^2×10^3) for exp_1386_HCQ. U_{eq} is defined as 1/3 of of the trace of the orthogonalised U_{IJ} tensor.

Atom	*x*	*y*	*z*	U(eq)
O2	4503.0(7)	4067.3(13)	5746.4(8)	28.7(3)
O002	3929.0(7)	3856.1(13)	7206.9(8)	29.4(3)
O1	5445.1(7)	6600.6(14)	6689.0(7)	29.9(3)
O3	3630.4(7)	10431.7(14)	4796.6(8)	32.6(3)
N2	4273.1(8)	5696.6(15)	5527.2(8)	23.5(3)
N3	5428.2(9)	10935.8(17)	6689.4(9)	31.4(3)
C7	3563.5(9)	6002.4(19)	4763.2(10)	23.5(3)
C8	3335.1(9)	7644.4(19)	4493.9(9)	24.3(3)

C9	5016.5(9)	9902.0(18)	6254.4(10)	25.8(3)
C3	2623.3(9)	8010(2)	3726.8(10)	29.6(4)
C6	3064.5(10)	4707.5(19)	4259.4(11)	28.6(3)
C5	2362.5(10)	5087(2)	3503.7(11)	32.9(4)
C4	2141.3(10)	6727(2)	3232.5(11)	34.1(4)
N1	3834.1(8)	8943.8(15)	5015.6(8)	24.1(3)
C1	4801.0(9)	6884.0(18)	6033.2(10)	23.4(3)
C2	4525.7(9)	8564.2(18)	5741.4(10)	23.9(3)

Table 3 Anisotropic Displacement Parameters ($Å^2 \times 10^3$) for exp_1386_HCQ. The Anisotropic displacement factor exponent takes the form: -$2\pi^2[h^2a^{*2}U_{11}+2hka^*b^*U_{12}+\ldots]$.

Atom	U_{11}	U_{22}	U_{33}	U_{12}	U_{13}	U_{23}
O2	35.6(6)	18.4(5)	30.8(6)	3.5(4)	7.5(4)	3.5(4)
O002	29.8(6)	25.7(6)	28.9(6)	-1.8(4)	2.9(4)	0.9(4)
O1	28.3(5)	27.2(6)	29.0(6)	-0.9(4)	0.1(4)	3.1(4)
O3	39.9(6)	21.8(6)	37.1(6)	7.4(4)	13.1(5)	6.6(4)
N2	25.6(6)	19.0(6)	24.9(6)	1.3(4)	5.7(5)	2.7(4)
N3	40.9(7)	25.7(7)	29.6(7)	-3.6(5)	13.3(6)	-3.5(5)
C7	22.5(7)	27.3(8)	21.6(7)	0.4(5)	7.9(5)	1.2(5)
C8	24.1(7)	27.4(8)	22.8(7)	1.3(5)	8.8(5)	1.1(5)
C9	31.4(7)	24.3(7)	24.1(6)	1.0(6)	12.1(5)	1.0(5)
C3	26.5(7)	36.0(9)	26.6(7)	5.5(6)	8.2(6)	6.0(6)
C6	27.8(7)	29.4(8)	28.6(7)	-2.4(6)	8.5(6)	-2.2(6)
C5	27.5(7)	43.2(9)	27.0(7)	-5.5(6)	6.6(6)	-6.1(6)
C4	24.9(7)	50.6(10)	24.8(7)	2.3(7)	4.2(6)	1.1(6)
N1	26.7(6)	22.3(6)	25.6(6)	2.6(5)	11.2(5)	3.0(4)
C1	24.3(7)	23.8(7)	22.6(6)	-0.3(5)	7.6(5)	1.4(5)
C2	27.3(7)	22.3(7)	23.2(7)	-1.0(5)	9.2(6)	0.5(5)

Table 4 Bond Lengths for exp_1386_HCQ.

Atom	Atom	Length/Å	Atom	Atom	Length/Å
O2	N2	1.3810(16)	C8	C3	1.3973(19)
O1	C1	1.2262(18)	C8	N1	1.4117(19)
O3	N1	1.2637(16)	C9	C2	1.425(2)
N2	C7	1.3831(18)	C3	C4	1.375(2)
N2	C1	1.3592(19)	C6	C5	1.381(2)
N3	C9	1.145(2)	C5	C4	1.400(3)
C7	C8	1.403(2)	N1	C2	1.3462(19)
C7	C6	1.400(2)	C1	C2	1.455(2)

Table 5 Bond Angles for exp_1386_HCQ.

Atom	Atom	Atom	Angle/°	Atom	Atom	Atom	Angle/°
C7	N2	O2	117.87(12)	C4	C5	C6	121.65(15)
C1	N2	O2	117.24(11)	C5	C4	C3	120.09(14)
C1	N2	C7	124.68(12)	C8	N1	O3	120.04(12)
C8	C7	N2	119.32(13)	C2	N1	O3	121.15(13)
C6	C7	N2	121.31(14)	C2	N1	C8	118.81(12)
C6	C7	C8	119.37(13)	N2	C1	O1	124.32(13)
C3	C8	C7	121.23(14)	C2	C1	O1	121.87(13)
N1	C8	C7	119.01(12)	C2	C1	N2	113.80(12)
N1	C8	C3	119.76(14)	N1	C2	C9	117.51(13)
C2	C9	N3	177.52(16)	C1	C2	C9	118.21(13)
C4	C3	C8	118.88(15)	C1	C2	N1	124.28(13)
C5	C6	C7	118.77(15)				

Table 6 Hydrogen Atom Coordinates (Å×10^4) and Isotropic Displacement Parameters (Å^2×10^3) for exp_1386_HCQ.

Atom	*x*	*y*	*z*	U(eq)
H2	4355(13)	3776(8)	6223(10)	43.1(4)
H00a	4180(9)	4607(18)	7593(12)	44.1(4)
H00b	3395.7(17)	3950(20)	7101(14)	44.1(4)
H3	2474.8(9)	9126(2)	3549.7(10)	35.5(4)
H6	3206.1(10)	3588.1(19)	4434.2(11)	34.3(4)
H5	2021.0(10)	4214(2)	3159.1(11)	39.5(5)
H4	1657.6(10)	6954(2)	2706.3(11)	40.9(5)

Experimental

The crystals of $C_9H_7N_3O_4$ [exp_1386_HCQ] were obtained as deep red rods from ethanol solution. The single-crystal XRD data collection and data reduction were performed using CrysAlis PRO on a single-crystal Rigaku Oxford XtaLab Pro diffractometer. The crystal was kept at 93 K during data collection. Using Olex2 [1], the structure was solved with the ShelXT [2] structure solution program using Intrinsic Phasing and refined with the olex2.refine [3] refinement package using Gauss-Newton minimization.

1. Dolomanov, O.V., Bourhis, L.J., Gildea, R.J, Howard, J.A.K. & Puschmann, H. (2009), J. Appl. Cryst. 42, 339-341.
2. Sheldrick, G.M. (2015). Acta Cryst. A71, 3-8.
3. Bourhis, L.J., Dolomanov, O.V., Gildea, R.J., Howard, J.A.K., Puschmann, H. (2015). Acta Cryst. A71, 59-75.

Crystal structure determination of [exp_1386_HCQ]

Crystal Data for $C_9H_7N_3O_4$ (M =219.18 g/mol): monoclinic, space group C2/c (no. 15), a = 16.4937(3) Å, b = 8.07760(10) Å, c = 14.6807(3) Å, β = 107.189(2)°, V = 1868.54(6) Å^3, Z = 8, T = 93 K, μ(Cu Kα) = 1.091 mm^{-1}, *Dcalc* = 1.5723 g/cm^3, 4615 reflections measured (11.24° ≤ 2Θ ≤ 159.14°), 1954 unique (R_{int} = 0.0197, R_{sigma} = 0.0272) which were used in all calculations. The final R_1 was 0.0450 (I>=2u(I)) and wR_2 was 0.1405 (all data).

Table S12. Tabular column for previously reported molecules depicting N-oxide ESIPT

S.No.	Structure	Reference
1.	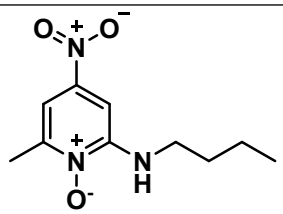	2-6
2.	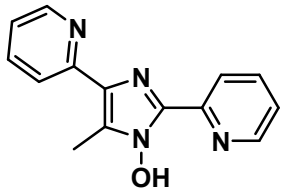	7-12
3.	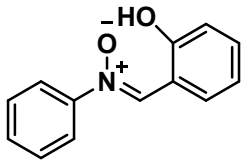	13

Table S13. Tabular column for previously reported organic fluorophores utilised for water detection:

S.No.	Structure	Mechanism	Reference
1.	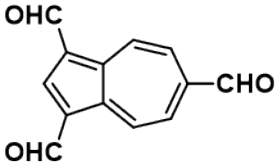	H-bonding between formyl groups and water leading to S_2-to-S_0 emission	[14]
2.	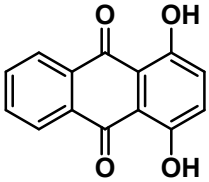	Anion-induced deprotonation followed by re-protonation with water	[15]
3.	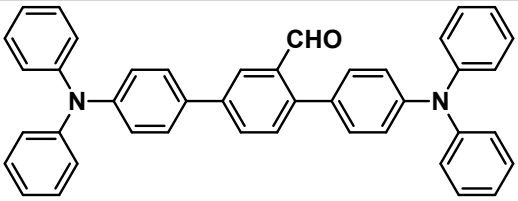	Solvent polarity as and hydrogen-bonding interactions	[16]
4.	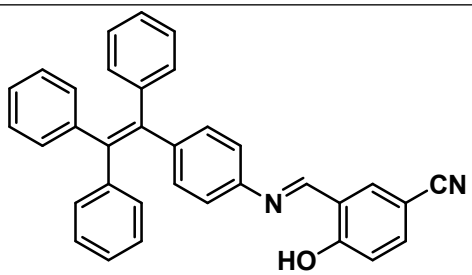	ESIPT	[17]
5.	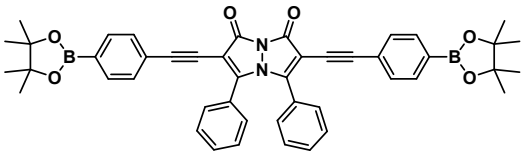	Hydrolysis of boronate ester	[18]
6.	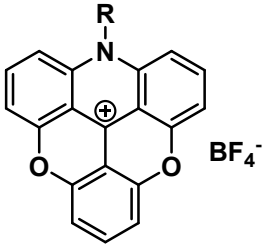	Water behaves as proton acceptor in a proton coupled electron transfer leading to quenching	[19]

Table S14. Tabular column for recently reported N-oxide fluorophores and their application.

S.No.	Structure	Application	Reference
1.	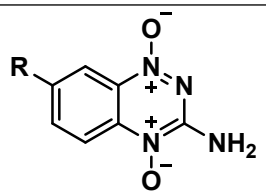	Detection of enzymes involved in hypoxia selective cytotoxin activation	[20]
2.	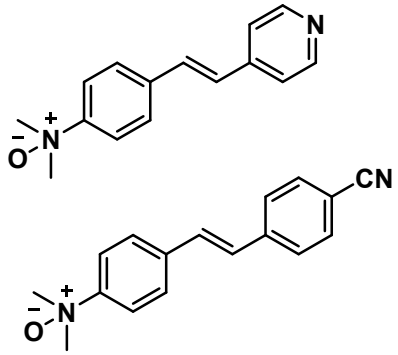	Heme and ferroptosis detection	[21]
3.	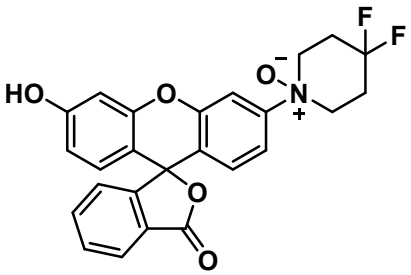	Labile Heme imaging in live cells	[22]
4.	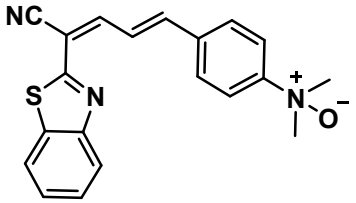	Fe^{2+} sensing	[23]
5.	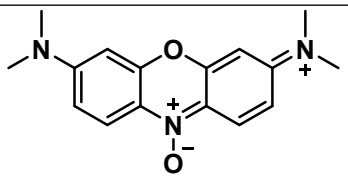	Nitric oxide detection	[24]
6.	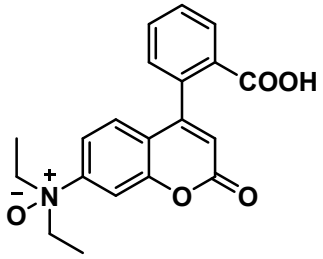	Bilirubin detection in human blood serum	[25]
7.	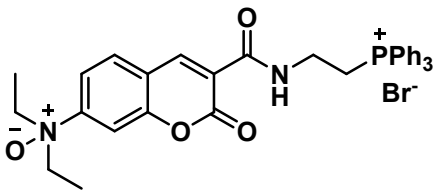	Fe^{2+} detection in cosmetics and live cells	[26]

8.	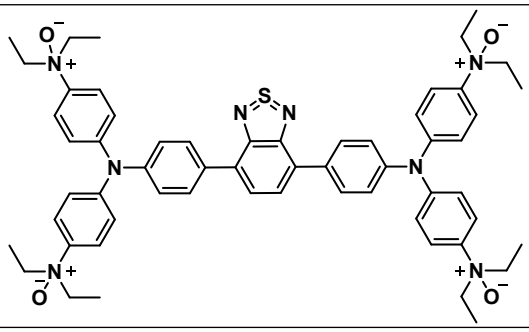	Hypoxia detection and tumor imaging	27
9.	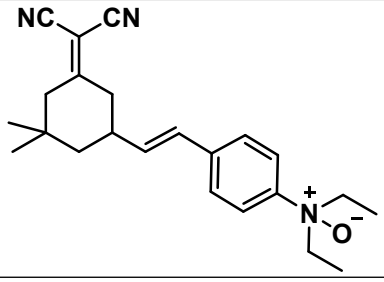	Fe^{2+} sensing and bioiimaging	28
10.	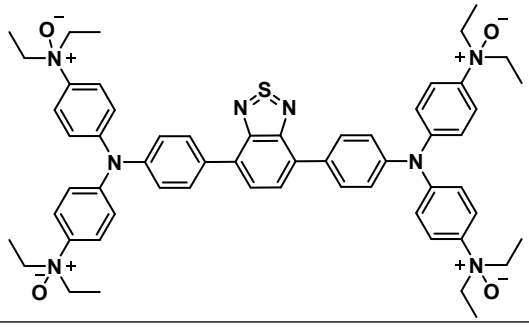	Fe^{2+} and H^{+} detection	29

References:

1. Lakowicz, J. R., *Principles of fluorescence spectroscopy*. Springer: 2006.
2. Szemik-Hojniak, A.; Deperasiñska, I.; Jerzykiewicz, L.; Sobota, P.; Hojniak, M.; Puszko, A.; Haraszkiewicz, N.; van der Zwan, G.; Jacques, P., Crystal Structure, Spectroscopic, and Theoretical Investigations of Excited-State Proton Transfer in the Doubly Hydrogen-Bonded Dimer of 2-Butylamino-6-methyl-4-nitropyridine N-Oxide. *The Journal of Physical Chemistry A* **2006,** *110* (37), 10690-10698.
3. Klerk, J. d.; van Stokkum, I. H.; Szemik-Hojniak, A.; Deperasinska, I.; Gooijer, C.; Zhang, H.; Buma, W.-J.; Ariese, F., Excited state processes of 2-butylamino-6-methyl-4-

nitropyridine N-oxide in nonpolar solvents. A transient absorption spectroscopy study. *The Journal of Physical Chemistry A* **2010,** *114* (12), 4045-4050.
4. Poór, B.; Michniewicz, N.; Kállay, M.; Buma, W. J.; Kubinyi, M.; Szemik-Hojniak, A.; Deperasiñska, I.; Puszko, A.; Zhang, H., Femtosecond Studies of Charge-Transfer Mediated Proton Transfer in 2-Butylamino-6-methyl-4-nitropyridine N-Oxide. *The Journal of Physical Chemistry A* **2006,** *110* (22), 7086-7091.
5. Szemik-Hojniak, A.; Wiśniewski, Ł.; Deperasińska, I.; Makarewicz, A.; Jerzykiewicz, L.; Puszko, A.; Erez, Y.; Huppert, D., The impact of solvent polarity on intramolecular proton and electron transfer in 2-alkylamino-4-nitro-5-methyl pyridine N-oxides. *Physical Chemistry Chemical Physics* **2012,** *14* (22), 8147-8159.
6. de Klerk, J. S.; Szemik-Hojniak, A.; Ariese, F.; Gooijer, C., Intramolecular Proton-Transfer Processes Starting at Higher Excited States: A Fluorescence Study on 2-Butylamino-6-methyl-4-nitropyridine N-Oxide in Nonpolar Solutions. *The Journal of Physical Chemistry A* **2007,** *111* (26), 5828-5832.
7. Shekhovtsov, N. A.; Nikolaenkova, E. B.; Berezin, A. S.; Plyusnin, V. F.; Vinogradova, K. A.; Naumov, D. Y.; Pervukhina, N. V.; Tikhonov, A. Y.; Bushuev, M. B., Tuning ESIPT-coupled luminescence by expanding π-conjugation of a proton acceptor moiety in ESIPT-capable zinc (II) complexes with 1-hydroxy-1 H-imidazole-based ligands. *Dalton Transactions* **2022,** *51* (39), 15166-15188.
8. Shekhovtsov, N. A.; Nikolaenkova, E. B.; Vorobyova, S. N.; Plyusnin, V. F.; Vinogradova, K. A.; Sukhikh, T. S.; Tikhonov, A. Y.; Bushuev, M. B., Luminescence of ESIPT-capable zinc (II) complexes with a 1-hydroxy-1 H-imidazole-based ligand: exploring the impact of substitution in the proton-donating moiety. *Dalton Transactions* **2023,** *52* (23), 8114-8134.
9. Shekhovtsov, N. A.; Ryadun, A. A.; Bushuev, M. B., Luminescence of a Zinc (II) Complex with a Protonated 1-Hydroxy-1H-imidazole ESIPT Ligand: Direct Excitation of a Tautomeric Form. *ChemistrySelect* **2021,** *6* (44), 12346-12350.
10. Shekhovtsov, N. A.; Nikolaenkova, E. B.; Berezin, A. S.; Plyusnin, V. F.; Vinogradova, K. A.; Naumov, D. Y.; Pervukhina, N. V.; Tikhonov, A. Y.; Bushuev, M. B., A 1-Hydroxy-1H-imidazole ESIPT Emitter Demonstrating anti-Kasha Fluorescence and Direct Excitation of a Tautomeric Form. *ChemPlusChem* **2021,** *86* (10), 1436-1441.
11. Shekhovtsov, N. A.; Vinogradova, K. A.; Vorobyova, S. N.; Berezin, A. S.; Plyusnin, V. F.; Naumov, D. Y.; Pervukhina, N. V.; Nikolaenkova, E. B.; Tikhonov, A. Y.; Bushuev, M. B., N-Hydroxy–N-oxide photoinduced tautomerization and excitation wavelength dependent luminescence of ESIPT-capable zinc(ii) complexes with a rationally designed 1-hydroxy-2,4-di(pyridin-2-yl)-1H-imidazole ESIPT-ligand. *Dalton Transactions* **2022,** *51* (25), 9818-9835.
12. Shekhovtsov, N. A.; Nikolaenkova, E. B.; Ryadun, A. A.; Samsonenko, D. G.; Tikhonov, A. Y.; Bushuev, M. B., ESIPT-Capable 4-(2-Hydroxyphenyl)-2-(Pyridin-2-yl)-1 H-Imidazoles with Single and Double Proton Transfer: Synthesis, Selective Reduction of the Imidazolic OH Group and Luminescence. *Molecules* **2023,** *28* (4), 1793.
13. Carneiro, L. M.; Keppler, A. F.; Ferreira, F. F.; Homem-de-Mello, P.; Bartoloni, F. H., Mechanisms for the Deactivation of the Electronic Excited States of α-(2-Hydroxyphenyl)-N-phenylnitrone: From Intramolecular Proton and Charge Transfer to Structure Twisting and Aggregation. *The Journal of Physical Chemistry B* **2022,** *126* (38), 7373-7384.
14. Zhou, Y.; Baryshnikov, G.; Li, X.; Zhu, M.; Ågren, H.; Zhu, L., Anti-Kasha's Rule Emissive Switching Induced by Intermolecular H-Bonding. *Chemistry of Materials* **2018,** *30* (21), 8008-8016.

15. Kumar, P.; Ghosh, A.; Jose, D. A., A simple colorimetric sensor for the detection of moisture in organic solvents and building materials: applications in rewritable paper and fingerprint imaging. *Analyst* **2019,** *144* (2), 594-601.
16. Huang, Z.; Tang, F.; Ding, A.; He, F.; Duan, R.-H.; Huang, J.; Kong, L.; Yang, J., D–A–D structured triphenylamine fluorophore with bright dual-state emission for reversible mechanofluorochromism and trace water detection. *Molecular Systems Design & Engineering* **2022,** *7* (8), 963-968.
17. Sun, H.; Sun, S.-S.; Han, F.-F.; Zhao, Y.; Li, M.-D.; Miao, B.-X.; Nie, J.; Zhang, R.; Ni, Z.-H., Water-stimuli-responsive dynamic fluorescent switch from Kasha's rule to anti-Kasha's rule based on a tetraphenylethene substituted Schiff base. *Chemical Engineering Journal* **2021,** *405*, 127000.
18. Pramanik, A.; Karmakar, J.; Grynszpan, F.; Levine, M., Highly sensitive water detection through reversible fluorescence changes in a syn-bimane based boronic acid derivative. *Frontiers in Chemistry* **2022,** *9*, 782481.
19. Jakobsen, R. K.; Laursen, B. W., New Principle for Simple Water Detection using Fluorescence Lifetime Triangulenium Probes. *ChemPhotoChem* **2024,** *8* (2), e202300215.
20. Shen, X.; Laber, C. H.; Sarkar, U.; Galazzi, F.; Johnson, K. M.; Mahieu, N. G.; Hillebrand, R.; Fuchs-Knotts, T.; Barnes, C. L.; Baker, G. A.; Gates, K. S., Exploiting the Inherent Photophysical Properties of the Major Tirapazamine Metabolite in the Development of Profluorescent Substrates for Enzymes That Catalyze the Bioreductive Activation of Hypoxia-Selective Anticancer Prodrugs. *The Journal of Organic Chemistry* **2018,** *83* (6), 3126-3131.
21. Dubey, Y.; Mansuri, S.; Kanvah, S., Detecting labile heme and ferroptosis through 'turn-on' fluorescence and lipid droplet localization post Fe2+ sensing. *Journal of Materials Chemistry B* **2024,** *12* (20), 4962-4974.
22. Kawai, K.; Hirayama, T.; Imai, H.; Murakami, T.; Inden, M.; Hozumi, I.; Nagasawa, H., Molecular Imaging of Labile Heme in Living Cells Using a Small Molecule Fluorescent Probe. *Journal of the American Chemical Society* **2022,** *144* (9), 3793-3803.
23. Zeng, X.; Chen, J.; Yu, S.; Liu, Z.; Ma, M., A highly selective and sensitive "turn-on" fluorescent probe for Fe2+ and its applications. *Journal of Luminescence* **2022,** *250*, 119069.
24. Jenni, S.; Renault, K.; Dejouy, G.; Debieu, S.; Laly, M.; Romieu, A., In Situ Synthesis of Phenoxazine Dyes in Water: Application for "Turn-On" Fluorogenic and Chromogenic Detection of Nitric Oxide. *ChemPhotoChem* **2022,** *6* (5), e202100268.
25. Ahmmed, E.; Mondal, A.; Sarkar, A.; Chakraborty, S.; Lohar, S.; Saha, N. C.; Dhara, K.; Chattopadhyay, P., Bilirubin Quantification in Human Blood Serum by Deoxygenation Reaction Switch-Triggered Fluorescent Probe. *ACS Applied Bio Materials* **2020,** *3* (7), 4074-4080.
26. Khatun, S.; Biswas, S.; Binoy, A.; Podder, A.; Mishra, N.; Bhuniya, S., Highly chemoselective turn-on fluorescent probe for ferrous (Fe2+) ion detection in cosmetics and live cells. *Journal of Photochemistry and Photobiology B: Biology* **2020,** *209*, 111943.
27. Li, M.; Li, H.; Wu, Q.; Niu, N.; Huang, J.; Zhang, L.; Li, Y.; Wang, D.; Tang, B. Z., Hypoxia-activated probe for NIR fluorescence and photoacoustic dual-mode tumor imaging. *iScience* **2021,** *24* (3), 102261.
28. Zhu, M.; Zhao, Z.; Liu, X.; Chen, P.; Fan, F.; Wu, X.; Hua, R.; Wang, Y., A novel near-infrared fluorimetric method for point-of-care monitoring of Fe2+ and its application in bioimaging. *Journal of Hazardous Materials* **2021,** *406*, 124767.
29. Xu, W.; Wu, P.; Li, X.; Liu, S.; Feng, L.; Xiong, H., Two birds with one stone: A highly sensitive near-infrared BODIPY-based fluorescent probe for the simultaneous detection of Fe2+ and H+ in vivo. *Talanta* **2021,** *233*, 122601.